# THE DEVELOPMENT OF A VIBRATION TECHNIQUE FOR ESTIMATION OF NEUTRAL TEMPERATURE IN CONTINUOUSLY WELDED RAILROAD RAIL

BY

MICHAEL J. KOOB

AVIPC, University of Illinois at Urbana-Champaign, 2001
B.S., University of Illinois at Urbana-Champaign, 2003

THESIS

Submitted in partial fulfillment of the requirements
for the degree of Master of Science in Civil Engineering
in the Graduate College of the
University of Illinois at Urbana-Champaign, 2005

Urbana, Illinois

# ABSTRACT

## THE DEVELOPMENT OF A VIBRATION TECHNIQUE FOR ESTIMATION OF NEUTRAL TEMPERATURE IN CONTINUOUSLY WELDED RAILROAD RAIL

Michael J. Koob, B.S.
Department of Civil and Environmental Engineering
University of Illinois at Urbana-Champaign
Christopher P.L. Barkan, Ph.D., Advisor
Richard L. Weaver, Ph.D., Advisor

The management of neutral temperature in continuously welded rails (CWR) is a major activity for railways and has significant safety and economic implications. CWR undergoes large changes in longitudinal forces due to constrained thermally induced expansion and contraction associated with temperature changes that can cause several types of failure of the track structure. A method to rapidly, economically and reliably estimate the neutral temperature of rail would substantially improve railroads' ability to manage neutral temperature.

Current technologies for measurement of neutral temperature are reviewed and the basic theory for a new vibration-based technique that would permit estimation of neutral temperature is described. The technique is based on the fact that, at fixed frequency, compressive longitudinal force decreases flexural wavelengths, while tensile force increases them. The method uses laser vibrometry measurements in combination with analysis of the lateral bending wave of the rail and does not require rail profilometry. For the technique to provide accurate results, the vibration modes must remain stable during the scan.

Tests on rail and track showed that the stability of the vibration modes could be improved by allowing the structure to relax in the laboratory and by liberating locked-in

longitudinal forces in the field. Structural drifts can be accounted for by using multiple accelerometers that capture the vibration state of the rail throughout the test. Vibrations in the scan platform were minimized by developing a field unit that was supported by the ties where it was found that vibration induced by a shaker on the test rail is lowest.

A laboratory test of the theory was conducted on a circular rod at 23 loads between 0 and 25 kips tension. The contained load was estimated within eight kips of the actual load and had a standard deviation (SD) of 3.4 kips. The final load cases used a clamped shaker and four reference accelerometers and had a SD less than two kips.

Studies on unworn and worn rail shapes were conducted in the laboratory at 24 loads between 0 and 100 kips compression. Neutral temperature was estimated to within 11°F on unworn American Railway Engineering and Maintenance of Way Association (AREMA) 136RE rail (136 pounds per yard) with a SD of 7.3°F. Tests on worn AREMA 136RE rail found that neutral temperature could be estimated within 27° with a SD of 13°F. The lower accuracy on the unworn rail may have been due to inaccurate predictions of the torsional wave speed used during the analysis process and future research should address this question.

A prototype rail stress testing apparatus was developed and preliminary tests were conducted in the field on mainline trackage of a Class 1 railroad. The apparatus is portable, measures the absolute value of force in the rail, and is independent of residual stresses. To conduct a test anchors and fasteners must be removed on three crossties. Ultimately, the objective is to be able to estimate neutral temperature with ±5°F accuracy within 30 minutes.

*To*

*Vivienne Genereux*

# ACKNOWLEDGEMENTS

This work was supported by the Technology Scanning Program of the Association of American Railroads and the Transportation Research Board's High Speed Rail IDEA program. Field-testing was made possible through the efforts and contributions of the CN and BNSF Railways. The Anderson's grain distribution center provided a local facility for initial feasibility studies.

I would like to express sincere gratitude to Professors Christopher P.L. Barkan and Richard L. Weaver for their guidance during this study. I thank Jim Meister for his help on the project. I also thank the entire Railroad Engineering program for memorable experiences inside and outside of B118.

I wish to thank all those who contributed their time and effort. These include John Tuckett, Josh Orwick, Grzegorz Banas, Hank Lees Jr., Don Rhodes, and Bill Meador. I am also grateful for the spontaneity and professionalism of both the CEE and TAM machine shops.

I thank my family for being continual sources of inspiration and my parents for the many sacrifices they have made for me. I enjoy sharing in the resolution of my sisters to enjoy life to the fullest. Finally, I posthumously appreciate the work ethic my grandmother, Vivienne Genereux, instilled in me. Few achievements would have been possible without her lessons, for this reason I dedicate this work to her.

# TABLE OF CONTENTS

# LIST OF TABLES

# LIST OF FIGURES

# CHAPTER 1

# INTRODUCTION

## 1.1 Introduction

North American railroads today rely primarily upon continuous welded rail (CWR) in mainline tracks. CWR is composed of flash-butt welded strings nominally one-quarter mile long. Thermite or electric welds are used in the field to join the rail sections into stretches that may be up to several miles in length. Typically they are interrupted only by insulated joints that electrically isolate sections of track used for the signal system, or at turnouts or other special track work. Insulated joints (IJs) can be two miles apart or less depending on crossing signals, intermediate signals, or home signals (Tuckett, 2005). Although the steel is "interrupted" at the IJs, it is not considered an interruption for the purpose of stressing or destressing welded rail because the IJ offers little if any allowance for expansion or contraction (Tuckett, 2005).

CWR use has reduced overall maintenance costs and extended rail life (Hay, 1982). The main advantages of CWR include a longer rail life due to the elimination of joint wear and batter, savings in general track maintenance costs due to reduced dynamic loadings, and a smoother, quieter, running surface (Hay, 1982). Although CWR has been widely adopted by the railroad industry because of its overall cost savings, management

of longitudinal forces due in part to constrained thermal expansions and contractions, is estimated to cost the industry $134 million annually (Davis, 2003).

| $T_0$ Management Costs (Millions of Dollars) | |
|---|---|
| $15 | Track Buckle Repair |
| $28 | Buckle Derailments |
| $51 | Slow Orders |
| $40 | Destressing |
| $134 | Annually |

**Table 1.1 Annual $T_0$ Management Costs** *(Davis, 2003)*

CWR undergoes large changes in longitudinal forces due to constrained thermally induced expansion and contraction associated with temperature changes. Excessive compressive forces and weak ballast restraint can result in track-buckles (also referred to as sun-kinks) – the tendency of the track to suddenly snap into a large lateral displacement profile (Read *et al*., 2004). Excessive tensile forces can result in rail pull-aparts – breaks typically occurring at a weld where the rail is weakest (Green and Shrubsall, 2004). On average, track-buckles are responsible for 35 mainline derailments per year while pull-aparts cause about 80 mainline derailments per year in the United States (Anderson and Barkan, 2003).

**Figure 1.1 Compression and Tension Failures in Rail** *(photo by D. Uzarski, 2005)*

The temperature at which CWR is laid is referred to as the neutral temperature, $T_0$. When the rail temperature is equal to $T_0$ the net longitudinal force in the rail is zero. Rail temperatures greater than $T_0$ would cause the rail to expand, but because the rail is constrained longitudinally, a net compressive state results. Rail temperatures less than $T_0$ would tend to contract the rail, but the rail is similarly constrained longitudinally, therefore a net tension state results. In an attempt to keep the rail forces below values that could cause a track-buckle or a pull-apart, railroads specify a target rail laying temperature (TRLT) at installation. Most North American railroads set their TRLT at 95°F in Canada, and 105°F in the United States (Tuckett, 2005). The TRLT is intentionally set higher than the mean annual temperature to prevent the generation of excessively high buckling forces during the hottest summer months (Meador, 2004).

Despite efforts to set the rail installation temperature at the TRLT, $T_0$ does not remain constant over time because the rails may not be fully constrained. Elongation or contraction can occur whenever the track is subjected to train or thermally induced loads (Kish and Samavedam, 2005). For instance, train braking and traction forces can displace the rail longitudinally, inertial forces can push the rail in or out on curves, and certain track maintenance activities can alter the length of the rail (Kish *et al.*, 1987). Changes in the rail length have the effect of changing $T_0$.

The state of longitudinal force in the rail is elusive because $T_0$ does not remain constant after installation. Existing and proposed technologies have either not had the desired accuracy, or have been too cumbersome or time consuming to be universally practical for regular measurement of longitudinal rail forces.

## 1.2 Objectives of Study

There is a need in the railroad industry for a non-destructive technique to measure $T_0$. Weaver and Barkan (2000) proposed a guided-wave vibration technique for the non-destructive measurement of contained stress. The following objectives were specified by Kish and Samavedam (1987) as guidelines for the development of a technique that would *non-destructively* measure $T_0$ and have value to the railroad industry.

The technique was required to:

1. be *portable* and not permanently attached to the rails,
2. measure the *absolute value* of force instead of relative levels,
3. be *independent of residual stresses* in the rail,
4. and measure $T_0$ within $\pm 5°F$,

In addition, Weaver and Barkan (2000) aimed for tests to be performed within *30 minutes* and be *easily adaptable to different sizes and wear patterns of rail.* Currently available techniques satisfy some, but not all, of these criteria and none has been found sufficiently useful to North American Railroads when track-time is at a premium (Lees, 2005).

## 1.3 Conclusions

A practical, fast, accurate technique to measure $T_0$ is needed by the railroads that will enable them to efficiently monitor and manage changes in $T_0$. This thesis presents a vibration technique for estimating $T_0$ in CWR. I describe the basic theory, the experimental techniques, apparatus and results in laboratory and field tests, as well as the analytical and computational methods used.

# CHAPTER 2

# CONTINUOUSLY WELDED RAIL

## 2.1 Introduction

Bolted rail joints are generally considered the weakest unit of the railroad track structure. They require considerable maintenance and are the forerunner to many track ailments – worn joint bars, rail end batter, worn and pumping ties, and contribute to overall track deterioration (Hay, 1982). Although progress has been made by improving joint bars and hardening rail ends, the best answer is to eliminate the joint entirely. This has been accomplished by the widespread use of CWR particularly on high tonnage mainline trackage. Evidence of its benefits can be found in its rapid adoption by Class I railroads. In the twenty-five years from 1978 to 2003, total installed track miles of CWR on Class I railroads has increased from 16,452 miles to 103,868 miles (Association of American Railroads, 1978, 2003). CWR has many advantages over jointed rail with regard to improved safety, reduced maintenance, and improved ride quality; however, it introduces new safety and maintenance challenges as well.

## 2.2 Theory of Expansion

CWR can experience large compressive and tensile longitudinal forces due to temperature changes. In jointed rail the angle bars are designed to accommodate a certain amount of expansion and contraction at joints which are typically spaced every 39 ft (11.89 m). The longitudinal strain, $\varepsilon_l$, due to constrained thermal expansion and contraction can be calculated using the formula,

$$\varepsilon_l = \alpha\left(T_r - T_0\right) \tag{2.1}$$

where $\alpha$ is the coefficient of thermal expansion, typically taken as 6.5E-6 per degree Fahrenheit (°F) for steel. $T_r$ is the temperature of the rail and $T_0$ is the rail neutral temperature. A 1°F deviation from neutral temperature corresponds to a longitudinal strain,

$$\varepsilon_l = (6.5\text{E-}6/°\text{F})(1°\text{F}) = 0.0000065 \tag{2.2}$$

The longitudinal strain can be expressed as 0.412 in/mile (0.650 cm/km). The expansion is considerable considering a 100°F deviation from neutral temperature results in a 41.2 in/mile (65.0 cm/km) change in rail length.

In CWR (or jointed rail with seized joints) the longitudinal expansion or contraction of the rail is constrained so deviations in temperature result in longitudinal force, $P$, proportional to the longitudinal strain.

$$P = EA\varepsilon_l \tag{2.3}$$

where $E$ is the modulus of elasticity, for steel a constant 29,000 ksi and $A$ is the cross-sectional area of the rail. The American Railway Engineering and Maintenance of Way Association (AREMA) sets the standards for most railroad rail used in North America.

Rail size is defined in pounds per yard and two sizes commonly used in recent years are 115 lbs/yd and 136 lbs/yd (referred to as 115RE and 136RE respectively). For 136RE rail, which has a cross-sectional area of 13.41 $in^2$, a 1°F change in temperature corresponds to a 2.53 kip longitudinal force as follows,

$$P = (29{,}000\text{ksi})(13.41\text{in}^2)(0.0000065) = 2.53 \text{ kips.} \quad (2.4)$$

When $T_r$ is equal to $T_0$ there is no net longitudinal force in the rail. Rail temperatures below or above $T_0$ would cause the rail to longitudinally contract or expand, respectively. However, if this contraction or expansion is constrained, as is the case when the rail is properly anchored and fastened, a net state of longitudinal tension or compression will exist (Figure 2.1) and result in longitudinal force proportional to the deviation from neutral temperature (Figure.2.2).

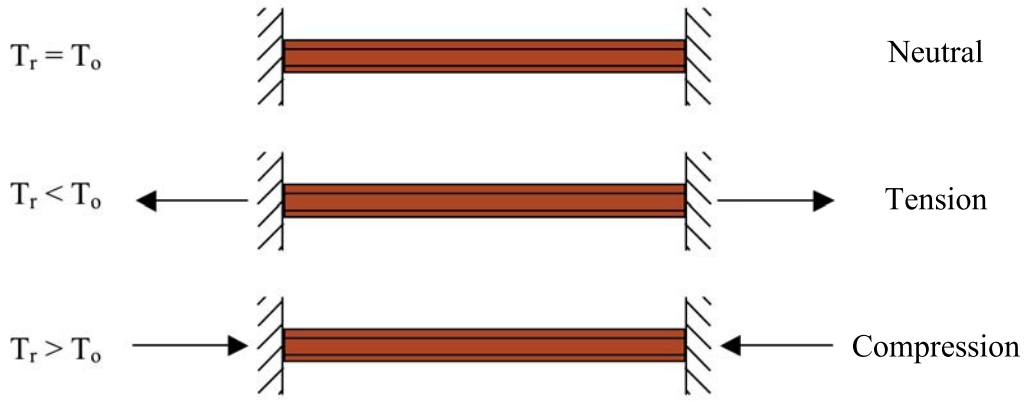


**Figure 2.1 States of Longitudinal Force in CWR**

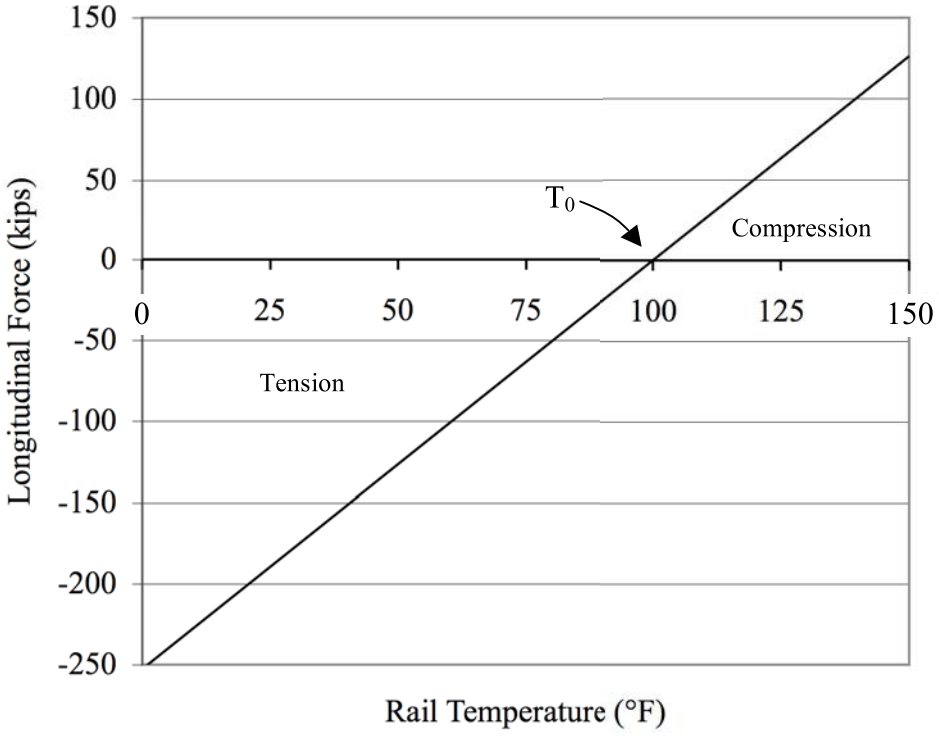


**Figure 2.2 Longitudinal Force in 136RE CWR**

## 2.3 Maintenance Practices

Zarembski, Grissom, and Lees (2004) have shown that the track buckling potential increases as neutral temperature falls below the TRLT. Conversely, a high neutral temperature can induce pull-aparts during cold temperatures. According to Kish and Samavedam (2005) railroad maintenance personnel currently rely on experience and guesswork to identify buckling or pull-apart prone locations requiring stress management practices.

Maintenance of CWR starts with an adequate ballast section and proper rail anchorage (Hay, 1982). To provide adequate lateral restraint to resist track buckling, full

cribs and an ample shoulder of clean, high-grade ballast is required (Selig and Waters, 1994). Rail anchors must be applied immediately after adjustment for laying temperature. To provide effective anchoring to resist temperature or train-movement-caused longitudinal forces, every other tie should be box anchored through the full length of the welded rail string (AREMA part 5.4.3, 2000).

Certain locations warrant the track maintainer's special attention. These include locations where rail could be drawn through the anchors by locomotive traction or train braking forces, such as on grades or at signals. "Hard" points in the track structure, such as diamonds, turnouts, and bridges, can block running of the rail and cause it to bunch, locally lowering $T_0$, or stretch, locally raising $T_0$. On curved track, spaces between the edges of ties and the ballast can indicate lateral shifting or breathing of the curve.

When a rail break or pull-apart occurs in winter it can be difficult to raise the rail temperature to the TRLT. In these circumstances many railroads will repair the break by welding or bolting in additional rail without setting the rail temperature as a temporary fix. This raises the local $T_0$ and so these locations must be properly reset to the TRLT before warmer weather causes a locally high risk of a track-buckle. In hot weather, lateral waviness (sometimes referred to as "kinky" rail) can indicate high longitudinal compressive forces in rail and may alert track maintenance personnel of an impending track-buckle condition.

## 2.4 Stressing

Readjustment of the longitudinal state of stress in the rail to set the rail neutral temperature is a maintenance procedure known as stressing. Destressing the rail involves subtracting steel from the rail. Restressing the rail involves pulling the rail back together to increase lost tension.

Destressing the rail involves cutting the rail, freeing the rail of anchors and fasteners for a specified length, adjusting the gap length to achieve the desired neutral temperature, welding the rail, and refastening it. Destressing the rail is the maintenance action performed when the rail neutral temperature is low or the rail is under large compressive forces. During the procedure steel is subtracted from the rail and $T_0$ is increased (Figure 2.3).

**Figure 2.3 Rail Destressing**

Restressing the rail involves the use of hydraulically powered rail clamps to pull the two rail sections together and then welding or bolting them to increase the rail tension (Figure 2.4). Restressing is the practice commonly used in cold weather where it would be difficult to provide the heat-energy required to set the desired $T_0$.

**Figure 2.4 Rail Restressing**

## 2.5 Conclusions

CWR eliminates the bolted rail joint, a weak and high maintenance element of the track structure. CWR is subjected to large forces because it is constrained longitudinally. These forces can result in failure of the rail or the track structure. The current industry maintenance and stressing practices would benefit by an ability to accurately estimate $T_0$.

# CHAPTER 3

# REVIEW OF TECHNOLOGIES FOR MEASUREMENT OF NEUTRAL TEMPERATURE

## 3.1 Introduction

There are several techniques currently available for assessing the state of longitudinal rail forces, but none of these fully satisfy Kish and Samavedam's (1987) criteria that the technique be non-destructive, portable, measure the absolute force in the rail, be independent of residual stresses, measure $T_0$ within ±5°F and Weaver and Barkan's (2000) criteria that the test be performed within 30 minutes and be easily adaptable to different size and wear patterns of rail. A review of the more promising techniques – strain gauge, rail uplift, ultrasonic, magnetic, and vibration – is presented in this chapter.

## 3.2 Strain Gauge

The use of strain gauges to measure strain in structural members is a common measurement technique. The strain gauge measures the strain, or change in length per unit length, of the member either mechanically or by means of electrical resistance

(Banas and Simsir, 2002). For strain gauges to measure neutral temperature in CWR, the gauges must be calibrated to a strain-free state (Zarembski, 1980).

The mechanical strain gauge uses two indentations spaced a fixed distance apart that are punched along the rail's neutral axis when it is unloaded (Zarembski, 1980). This procedure is done on both the rail and on a standard, usually a short segment of similar rail that is left in the field near the rail being measured. The standard is measured for thermally induced strain and the net strain in the standard (strain in the standard minus the strain in the rail) corresponds to the longitudinal stress experienced by the rail constrained in the track.

The electrical resistance strain gauge simplifies rail longitudinal strain measurement (Zarembski, 1980). The electrical resistance strain gauge can either be bonded or spot-welded to the neutral axis of the rail. More commonly spot-welded gauges (Figure 3.1) are used on rail because they are better suited for severe environments (Banas and Simsir, 2005).

**Figure 3.1 Spot-Welded Strain Gauge Installation**

The electrical resistance strain gauge installation typically utilizes a half Wheatstone-bridge circuit (Figure 3.2). The half Wheatstone-bridge circuit uses two strain gauges, G1 and G2 on each side of the rail, and two fixed resistors, R1 and R2. The voltage across the galvanometer is proportional to the change in gauge resistance, which is proportional to the change in strain in the rail.

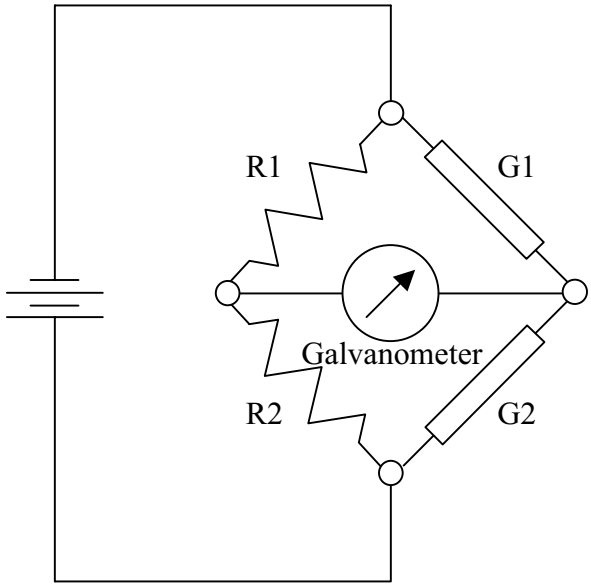


**Figure 3.2 Half Wheatstone-Bridge Circuit**

An advantage of the strain gauge technique is that temperature and rail lateral bending are compensated for (Kish *et al.*, 1987). Its use, however, requires cutting and destressing of the rail or the use or another technology to calibrate the gauges. Several companies specialize in strain gauge installations on CWR including DataTraks, Inc. and Salient Systems, Inc. This is probably the most commonly used technique to monitor $T_0$ in North America today.

### 3.3 Rail Uplift

The rail uplift technique is based on simple beam-column bending theory; namely the vertical force required to lift a rail varies with the axial force contained within the rail (Kish and Samavedam, 1987). The Transportation Technology Center (TTC) first demonstrated the concept in the early 1990s* using a track loading vehicle (Kish *et al*., 1993). The technology is currently marketed under the VERSE® (Vertical Rail Stiffness Equipment) name and is owned by Vortok International & AEA Technology based in the United Kingdom.

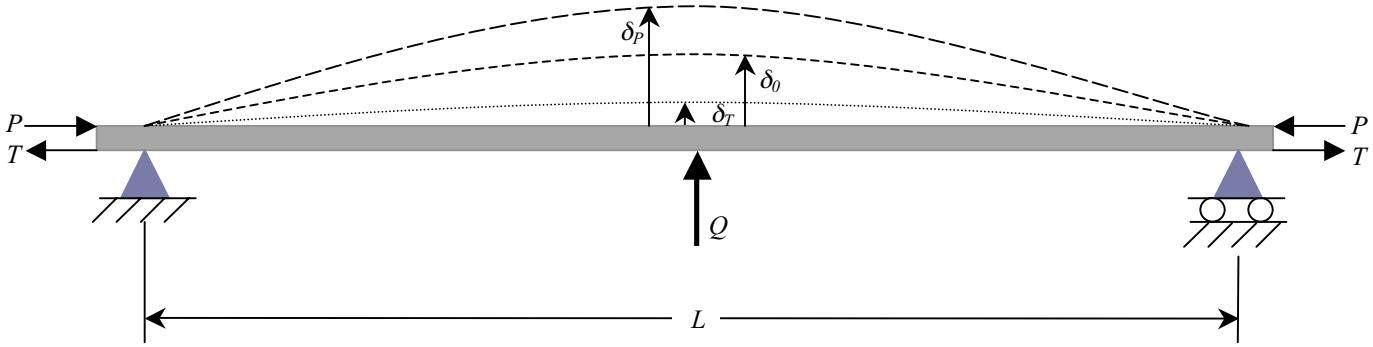


**Figure 3.3 Beam-Column Deflection Responses**

The VERSE® setup consists of a loading frame that is positioned over the rail to be measured. The frame lifts the rail by applying force, $Q$, while transducers measure the vertical displacement of the rail, $\delta$. The structure behaves like a beam-column; its deflection is measurably influenced by the longitudinal load in the rail (Kish and Samavedam, 1987). The compressive longitudinal load, $P$, will increase the deflection to $\delta_P$ at load $Q$ and the tensile longitudinal load, $T$, will decrease the deflection to $\delta_T$ for the same $Q$ (Vortok International and AEA Technology, 2004).

* Preliminary test conducted in August of 1986; see Kish and Samavedam, 1987.

Rail uplift $T_0$ results are calculated based on the load versus vertical displacement relationship. The relationship is given by,

$$\delta = \left( \frac{\lambda Q L^3}{EI} \right) \left( \frac{1}{1 - \frac{P}{P_C}} \right) \tag{3.1}$$

where $\lambda$ is a constant that depends on end constraints, $Q$ is the uplift force, $L$ is the unfastened rail length, and $EI$ is the stiffness of the rail. $P_c$ is the critical buckling load for the beam column over a length of $2L$. (The load-deflection relationship is linear for a fixed rail force. Equation 3.1, Figure 3.4.)

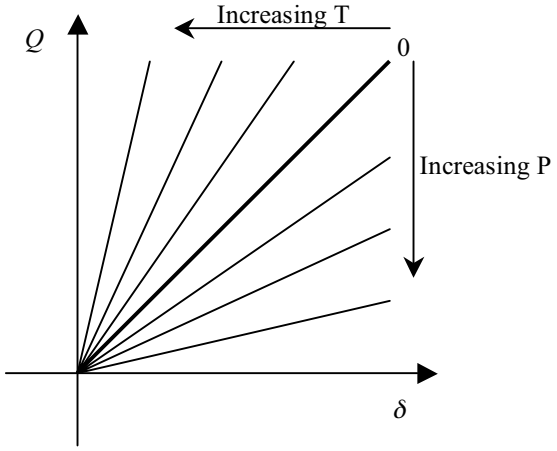


**Figure 3.4 *Q* vs. *d* Relationship for a Beam Column**

Rail uplift provides accurate results of $T_0$, however, the overall process is cumbersome. The lifted section of rail must be free of end effects; which requires that the rail must be unclipped for at least 35 yd (32 m). Riser blocks must also be added at the ends of the unclipped rail section to overcome the effects of friction.

Measurements using the rail uplift method are limited by an inability to test the rail under compression. The unfastened rail will easily bow under these circumstances therefore tests must be completed when the rail temperature is below $T_0$. Obvious difficulty arises when the rail temperature climbs above $T_0$ before the rail is replaced and refastened to the ties.

Curved track poses an additional complexity to the rail uplift method. While $T_0$ readings on curves are possible, tabulated correction values are needed to adjust for the chording effect of the rail. Again, replacing and refastening the rail is challenging.

VERSE® measurements require approximately 1 hour and 30 minutes per rail, which makes the technology well suited for routes where nighttime traffic is minimal such as many passenger and transit lines (Lees, 2005). Although, several North American freight railroads have recently adopted VERSE® for calibrating strain-gauged rails, the lengthy track time and requirement that the rail be in tension when taking measurements, imposes some limits on its utility.

### 3.4 Ultrasound

Ultrasound techniques are commonly used in the analysis and characterization of mechanical stress states because wave velocities depend on physical properties of the propagation medium (Si-Chaib *et al.*, 2001). It is well known that ultrasound velocity is changed by the stresses in a metal (Si-Chaib *et al.*, 2001). The first application of ultrasound to measure stress by the railroad industry dates back more than 30 years when the technology was used to measure residual stresses in wheels (Szelazek, 1998).

The propagation characteristics of ultrasound waves depend on physical properties, such as the volume density, the elastic constants, and the deformation of the propagation medium resulting from applied and/or residual stresses present inside the material (Si-Chaib *et al.*, 2001). Proposed ultrasonic techniques are based on propagation of ultrasonic waves that are either a measurement of acoustic birefringence or longitudinal wave propagation along the rail (Szelazek, 1998).

The acoustic birefringence technique involves probing the rail head and pulsing waves downward from the rail head to the rail base. The difference in flight times of pulses polarized along and perpendicular to the rail axis is proportional to the longitudinal force in the rail and the average value of residual stresses (Szelazek, 1998). If the anisotropy due to texture and the influence of residual stresses on measured times of flight are known, then the stress, $\sigma$, can be computed by,

$$\sigma = \frac{B_o - B_s}{\beta_B} \tag{3.2}$$

where $B_o$ is the ultrasonic anisotropy due to texture and residual stresses, $B_s$ is the thermal-stress-induced anisotropy, and $\beta_B$ is the elastoacoustic constant computed by,

$$\beta_B = \frac{1}{2}\left(\frac{t_L - t_P}{t_L + t_P}\right) \tag{3.3}$$

The values of $t_L$ and $t_P$ are the times of flight in the longitudinal and perpendicular polarization directions respectively.

The limitation of the acoustic birefringence method is that the effect of rail texture anisotropy and residual stresses on flight times must be known at the sampling point, that is, $B_o$ and $B_s$ must be known.

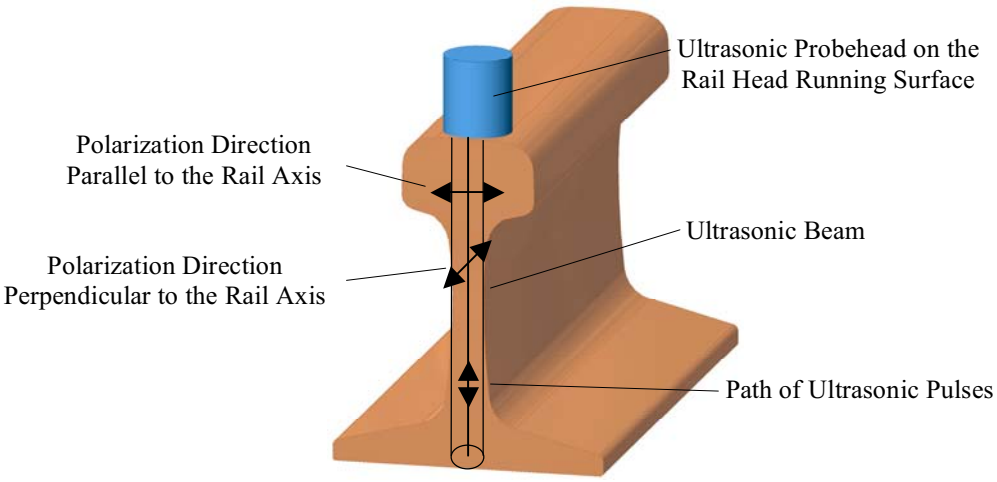


**Figure 3.5 Acoustic Birefringence Method in Rail**

A similar technique involves measuring the velocity of longitudinal waves in the rail. The velocity of longitudinally propagated waves is sensitive to longitudinal stress, but is also influenced by residual stresses and texture (Szelazek, 1998). Therefore estimates of $T_0$ can only be recovered if it is assumed that residual stresses and acoustic properties of the rail are constant (Szelazek, 1998).

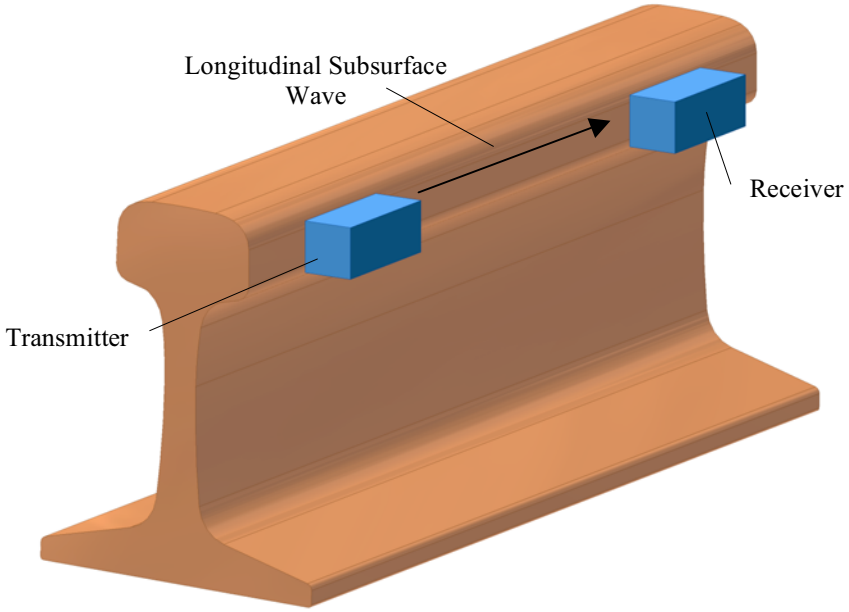


**Figure 3.6 Longitudinal Wave Propagation Method in Rail**

### 3.5 Magnetic

A magnetic technique has recently been studied as a continuous measurement system that would be able to identify variations of $T_0$ along the track (Wegner, 2005). The technique is based on Barkhausen noise effects in which jumps of magnetic flux are created as grains reorient themselves parallel to a magnetic field.

When magnetic grains in a ferrous material are subjected to a directional magnetic field they undergo a progression of changes in orientation as a function of the strength of the magnetic field. Initially they are aligned with no net magnetized direction, but as the strength of the magnetic field increases, the grains begin to align themselves with the direction of the magnetic field until finally, all of the grains are aligned (Figure 3.7).

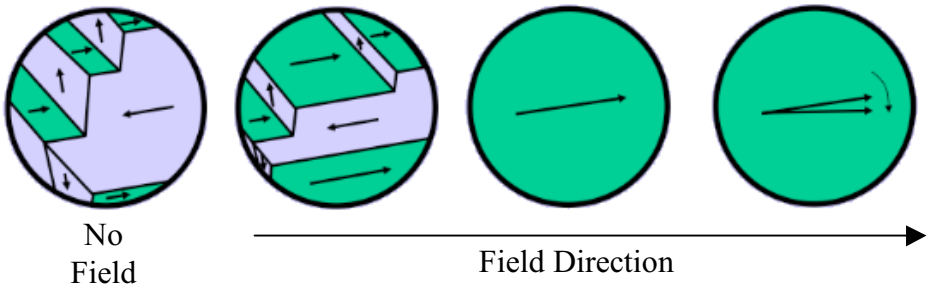


**Figure 3.7 Grain Reorientation in a Magnetic Field** *(Wegner, 2005)*

Lo *et al.* (2004) showed magnetic measurements can be used to nondestructively detect stress concentrations in magnetic materials. A prototype unit has recently been developed to attempt to apply this technique to rail (Wegner, 2005). The technique measures a hysteresis loop of a series of Barkhausen jumps that are created by the domain walls becoming pinned and released along grain boundaries under a smoothly changing magnetic field (Figure 3.8).

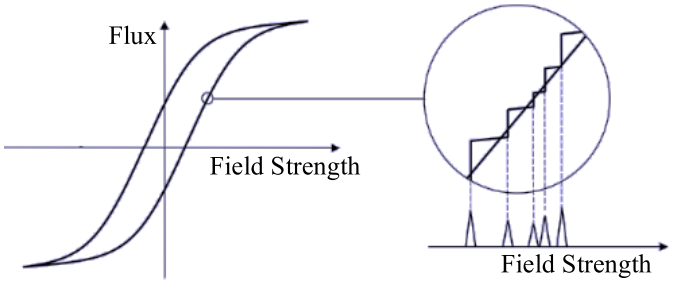


**Figure 3.8 Magnetic Hysteresis Loop of Barkhausen Jumps** *(Wegner, 2005)*

The Villari effect – changes in the magnetic permeability of the rail – and the magnitude of the Barkhausen noise are stress dependent (Wegner, 2005). Under compressive stress the hysteresis loop shows a decrease in magnetic permeability and a decrease in magnitude of Barkhausen noise – effectively stretching the hysteresis loop (Hauk, 1997). Tensile stresses increase the magnetic permeability of the rail and increase the magnitude of Barkhausen noise, which has the effect of compressing the hysteresis loop (Figure 2.9).

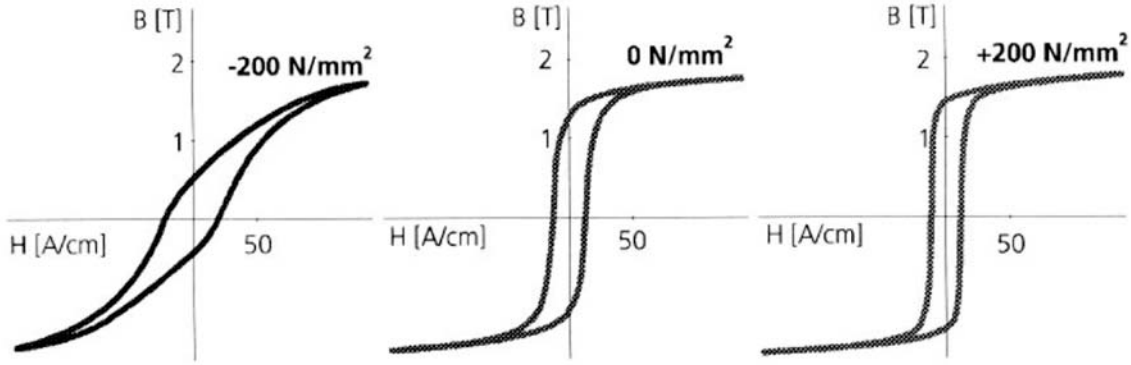


**Figure 3.9 Effect of Stress on Hysteresis Loop** *(Hauk, 1997)*

Recent application of the technology under laboratory loading conditions and on clean test specimens has been unsuccessful at quantifying the stress because the

relationship between the shape of the hysteresis loop (Figure 3.9) and state of stress is not yet well understood (Tsuchida and Enokizono, 2003). Tsuchida and Enokizono (2003) have suggested use of chaos theory to analyze magnetic signals as nonlinear ones to quantify this relationship.

Magnetic techniques are sensitive to rail texture; therefore to infer stress in a particular rail specimen, a calibration curve must be made for a rail with similar wear and residual stress patterns (Wegner, 2005). Preliminary tests by German investigators have required 400 laboratory samples to develop a calibration curve for a given 3 m section of rail (Wegner, 2005). Eventually a catalogue of rail profiles and residual stress states could be built with the hope that the operator would be able to select a calibration curve based on the field condition of the rail. The method's sensitivity to changes of wear and residual stress patterns along the length of the rail has not yet been studied.

### 3.6 Vibration

The most promising techniques so far involve vibration. Longitudinal force affects beam vibration just as it does on stringed musical instruments (Figure 3.10). The vibration response of the beam is sensitive to longitudinal force and intrinsic properties of the beam, but insensitive to residual stress and microstructure. There is no need for calibration because vibration techniques can determine the absolute state of stress in the rail.

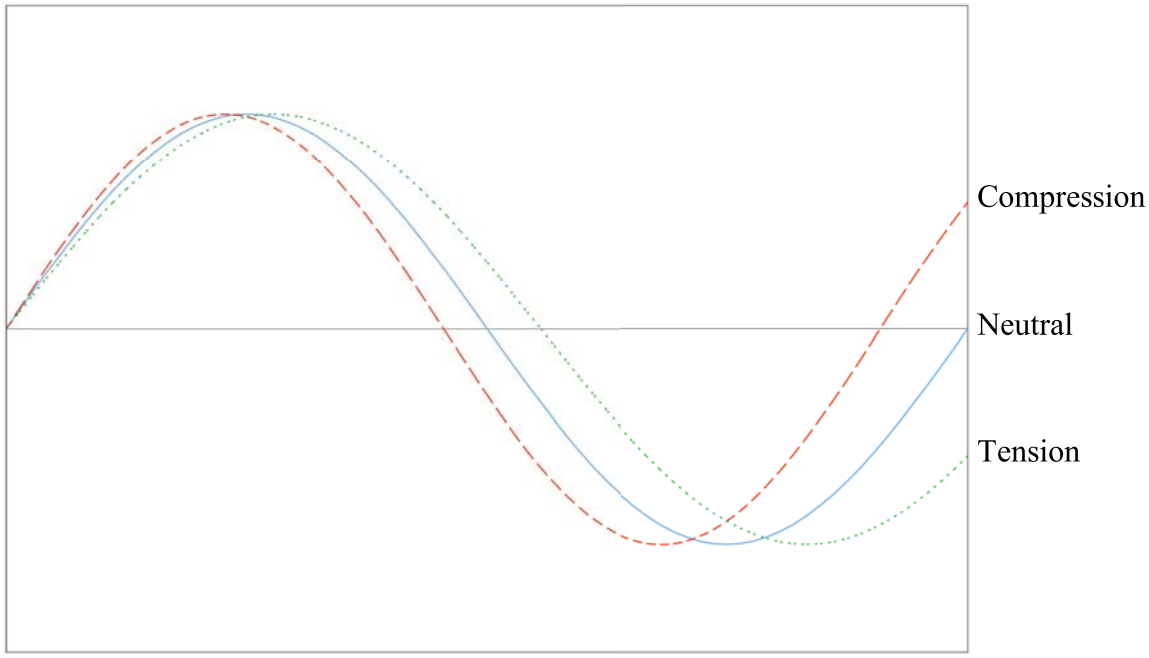


**Figure 3.10 Effects of Longitudinal Force on Wavelength**

Boggs *et al*. (1994) attempted to use vibration analyses to determine longitudinal force in continuous beams. Livingston *et al*. (1995) proposed modeling beam end conditions with translational and rotational springs. In both studies the resonant frequencies of response to a transient excitation were used to attempt to infer longitudinal force. However, while natural frequencies are sensitive to contained forces, they are also affected by variability in the supports, thus Boggs *et al.* (1994) and Livingston *et al.* (1995) were unable to reliably infer contained longitudinal force in the beams.

Béliveau and Murray (1996) attempted to determine longitudinal force in rail but were unable to do so consistently because their technique was similarly sensitive to variability in the supports.

# CHAPTER 4

# PROPOSED VIBRATION TECHNIQUE

## 4.1 Introduction

The use of vibration techniques for rail stress assessment is based on the effect of longitudinal force on the free vibrations of beams. It has been previously considered for this application but not successfully implemented (Béliveau and Murray, 1996). Compressive stresses decrease the flexural frequencies while tensile forces increase them (Weaver *et al.*, 1990). Past efforts to apply this principle for rail stress measurement have failed due to an inability to control or adequately measure other parameters, most particularly the location and stiffness of the supports (Boggs *et al.*, 1994, Livingston *et al.*, 1995, Béliveau and Murray, 1996).

## 4.2 Theory of Vibration Measurement of Contained Stress

Weaver and Barkan (2000) proposed a vibration technique that takes advantage of the known sensitivity of bending vibrations to contained longitudinal stress and is independent of the variability of supports. The approach allows for determination of rail stress from the wavelengths of vibration modes without the need to control boundary conditions.

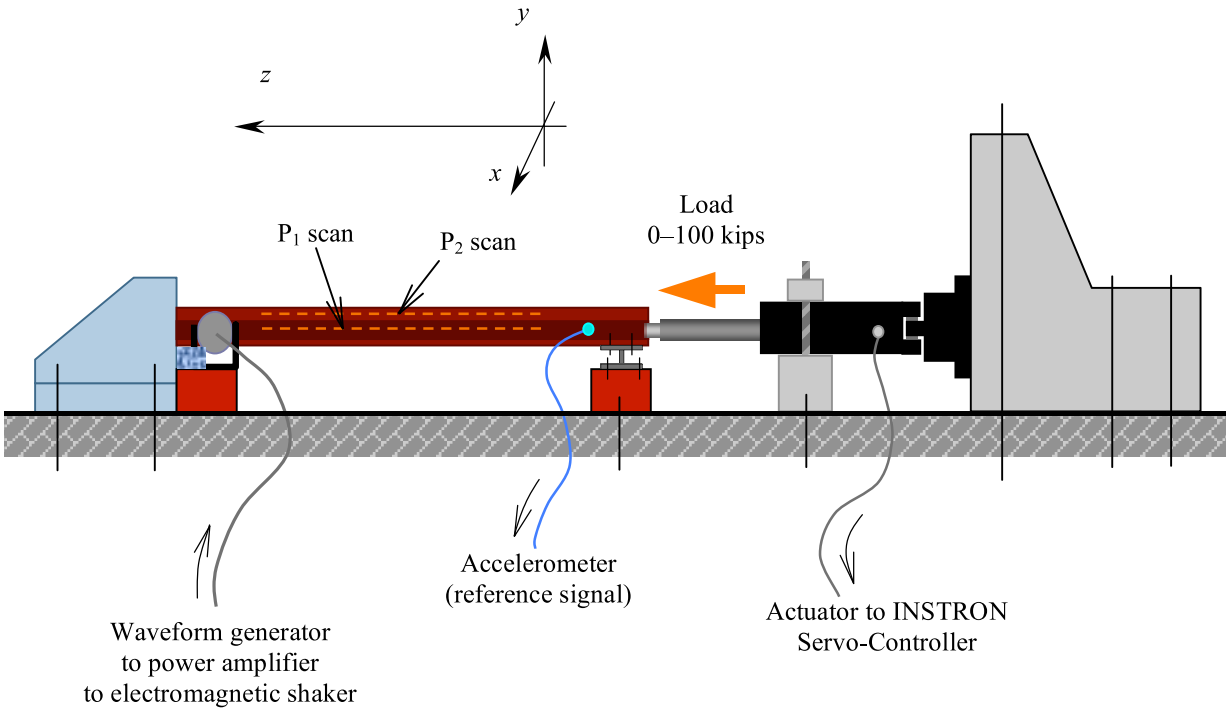


**Figure 4.1 Damljanovic Laboratory Setup** *(Damljanovic, 2003)*

Damljanovic (2003) conducted laboratory tests to infer axial stress in 136RE rail by vibrating the sample laterally (about the weak axis – the mode most affected by longitudinal stress). A frequency at or near a natural frequency in the resonant frequency spectrum was chosen to generate larger amplitude responses. An INSTRON hydraulic actuator loaded the rail longitudinally up to 100 kips and allowed for controlled, repeatable experiments. An accelerometer provided a reference vibration signal while a laser vibrometer scanned the displacements of discrete points along two heights on the rail's surface. The scanned displacement profile was then fit to the vibration modes obtained in a finite element analysis (FEA) of the rail. In Damljanovic's analysis, the actual dynamic displacement measurement of the rail, $\{\overline{A}\}$, was represented as the sum of the $M$ leftward and rightward bending waves for each location, $z$, along the longitudinal axis of the rail.

$$\left\{\overline{\mathsf{A}}\right\} = \sum_{m=1}^{M} \alpha_m \left\{\upsilon_m\left(x, y; \omega\right)\right\} e^{i\omega t - ik_m z} \tag{4.1}$$

where $\left\{\upsilon_m\left(x, y; \omega\right)\right\}$ is the $m^{\text{th}}$ guided mode shape at frequency $\omega$ and Cartesian coordinates (*x,y*), and $k_m$ is the is the $m^{\text{th}}$ wavenumber (Wavenumber $k = \frac{2\pi}{\lambda}$ where $\lambda$ is the wavelength) , which is dependent on the rail properties as well as on the contained load. This representation is valid with constant coefficients, $\alpha_m$, over any span in which the rail has uniform properties. Lateral bending modes dominated the sum because the excitation was applied in the lateral direction (Damljanovic, 2003).

The least-square residual between the measurement and the sum in Equation 3.1 was minimized in such a way that only the wavenumber of the particular lateral bending mode was allowed to vary, while all the other wavenumbers remained fixed. The longitudinal stress in the rail was then inferred based on the hypothesis that the percent change in lateral bending wavenumber, $\delta$, due to the contained load, *P*, is linear (Damljanovic, 2003, p.7).

Damljanovic (2003) observed a linear relationship between $\delta$ and *P* in a laboratory study based on four different load cases (Figure 4.2). The points are nearly collinear; however, Damljanovic (2003) noted an intercept error of about 0.36%. That is, her finite element code incorrectly estimated the zero-load bending wavenumber for unworn 136RE rail.

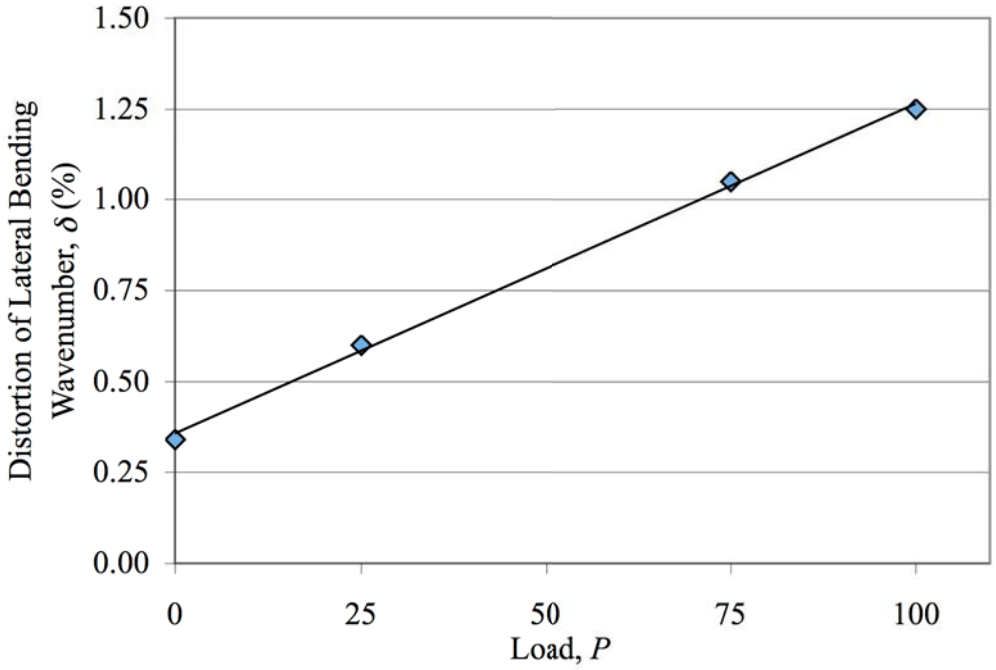


**Figure 4.2 Distortion of Lateral Bending Wavenumber versus Applied Load**
*(Damljanovic, 2003)*

Damljanovic (2003) concluded that longitudinal force affects the wavelength of bending waves and that the wavelengths can be inferred by comparing the vibration amplitude distributions with distributions based on the wavenumbers obtained by FEA. The technique was found to require a high-precision FEA for prediction of wavenumbers, to require an elaborate fitting procedure to the bending modes, and to require careful attention to sources of measurement error.

## 4.3 Two-Frequency Approach

Although the method used by Damljanovic (2003) was accurate in the laboratory, a limitation of the technique is its reliance on FEA for lateral bending wavenumber predictions. Field applications of the technique would require rail profilometry and a

FEA on the rail section. Although it might be possible to compare the measured rail profile to a cataloged set of various rail sizes with different wear patterns, the accuracy of such an approach is unknown and could pose practical difficulties to implement in the field.

The current approach for analysis is based on the Euler-Bernoulli effect of longitudinal load on the vibration of a prismatic beam. For this case, the governing differential equation for transverse vibrations, including inertial forces, is given as (Weaver *et al*., 1990),

$$EI\frac{\partial^4 v}{\partial x^4} - S\frac{\partial^2 v}{\partial x^2} = -\rho A\frac{\partial^2 v}{\partial t^2} \tag{4.2}$$

where $E$ is the modulus of elasticity, a constant; $I$ is the moment of inertia about the axis of vibration; $\rho$ is the unit density of the material, a constant; and $A$ is the cross-sectional area of the beam. $S$ is the longitudinal tension force. The solution is taken in the form,

$$v = X(A\cos\omega t + B\sin\omega t) \tag{4.3}$$

where $A$ and $B$ are constants and $X$ is a normal function. Substitution of Equation 4.3 into Equation 4.2 gives,

$$EI\frac{\partial^4 X}{\partial x^4} - S\frac{\partial^2 X}{\partial x^2} = \rho A\omega^2 X \tag{4.4}$$

The wavenumber, $k$, is introduced by taking $X$ equal to $e^{ikx}$, substituting, and then canceling the exponential terms. Equation 4.5 is the result,

$$EIk^4 + Sk^2 = \rho A\omega^2 \tag{4.5}$$

which can be reordered as,

$$\rho A\omega^2 = EIk^4 + Sk^2 \tag{4.6}$$

Dividing through by $\rho A$ and $k^2$ gives the most common dispersion relation equation,

$$\frac{\omega^2}{k^2} = \frac{EI}{\rho A}k^2 + \frac{S}{\rho A} \tag{4.7}$$

Equation 4.7 represents an equation of the form $y = mx + b$ when

$$y = \frac{\omega^2}{k^2} \qquad m = \frac{EI}{\rho A} \qquad x = k^2 \qquad b = \frac{S}{\rho A}$$

Furthermore, $\frac{EI}{\rho A}$ is identical to $r_g^2 c_{bar}^2$ where $r_g$ is the radius of gyration and $c_{bar}$ is dependent on the intrinsic properties of the rail, namely $c_{bar} = \sqrt{\frac{E}{\rho}}$. Finally, the equation of the line can be written as,

$$\frac{\omega^2}{k^2} = r_g^2 c_{bar}^2 k^2 + \frac{S}{\rho A} \tag{4.8}$$

If two driving frequencies, $\omega_1$ and $\omega_2$, are used to excite the beam and two wavenumbers, $k_1$ and $k_2$, are recovered from the analysis of the bending modes, a plot similar to Figure 4.3 can be drawn.

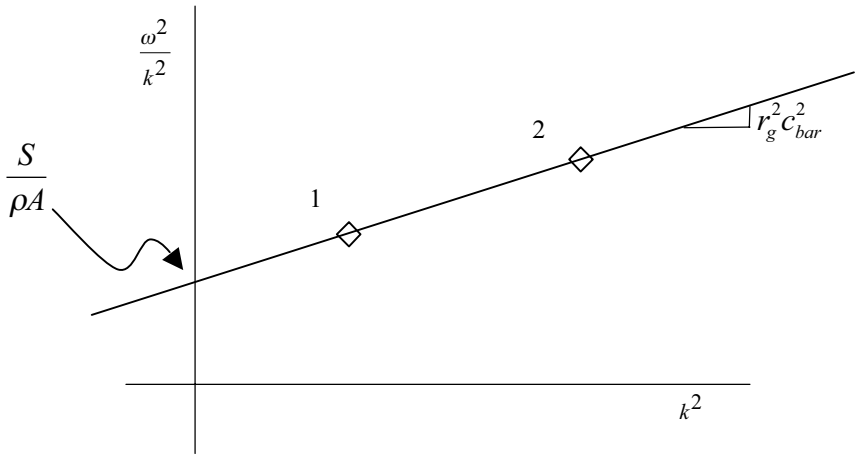


**Figure 4.3 Two-Frequency Approach**

The plot shown in Figure 4.3 is constructed with $\frac{\omega^2}{k^2}$ on the ordinate† and $k^2$ on the abscissa. Point 1 shown in Figure 3.4 is $\left(k_1^2, \frac{\omega_1^2}{k_1^2}\right)$ and point 2 shown in Figure 4.3 is $\left(k_2^2, \frac{\omega_2^2}{k_2^2}\right)$. The slope of the line through the two points is equal to $r_g^2 c_{bar}^2$. The intercept gives the value of $\frac{S}{\rho A}$. Provided the values of $\rho$ and $A$ are known or can be estimated to within 10%, the longitudinal load *S* can be extracted by this procedure. Neither $r_g^2$ nor $c_{bar}^2$ need to be known; rather, their product is recovered in the analysis.

So far the currently used approach has assumed that the cross-section of the beam is small in comparison with its length so that Euler-Bernoulli theory applies. However, for the theory to remain accurate on a short beam such as a segment of rail, the appropriate corrections to account for the effects of shear deformation and rotary inertia must be applied. Commonly referred to as the Timoshenko correction, Weaver *et al.* (1990) explain the effect of shear deformation and rotary inertia on the dispersion relation (Equation 4.8). The Timoshenko-corrected dispersion relation is then,

$$\omega_i = c_{bar} r_g k^2 \left[1 - \frac{1}{2} k^2 r_g^2 \left(1 + \frac{E}{k'G}\right)\right] \tag{4.9}$$

where *G* is the shear modulus and $k'$ is a numerical factor depending on the shape of the cross-section which can be estimated to sufficient accuracy. For steel, the ratio of *E* to *G*

† Alternatively, $\frac{f^2}{k^2}$ can be plotted where *f* is the frequency in the units Hz

is approximately $\frac{8}{3}$. If $r_g$ is not precisely known, as in the case of worn rail, the correction from approximate $k$ or $\omega$ can be obtained by noting,

$$k^2 r_g^2 = \frac{\omega^2}{c_{bar}^2 k^2} \tag{4.10}$$

Finally,

$$\omega_T = \omega_{EB}\left[1 - \frac{1}{2}\frac{\omega_{EB}^2}{c_{bar}^2 k^2}\left(1 + \frac{E}{k'G}\right)\right] \tag{4.11}$$

where $\omega_T$ is the Timoshenko frequency of vibration and $\omega_{EB}$ is the Euler-Bernoulli frequency of vibration ($\omega_{EB} = c_{bar} r_g k^2$). Using this technique, the measured frequency of vibration on the rail, $\omega_{EB}$, must be converted to $\omega_T$ per Equation 4.11 before using it in the fit of $\frac{\omega^2}{k^2}$ versus $k^2$to recover the load.

The result of an analysis by this procedure will recover the longitudinal load in the beam. In the case of CWR, where the objective is to find $T_0$, the load in the rail, *S*, can be equated to $T_0$ using Equation 4.12.

$$S = EA\alpha\left(T_0 - T_r\right) \tag{4.12}$$

where $\alpha$ is the coefficient of thermal expansion, and $T_r$ is the rail temperature at the time of the test.

# CHAPTER 5

# LABORATORY EXPERIMENTAL METHODS AND APPARATUS

## 5.1 Introduction

The accuracy and viability of the technique was tested in the laboratory and preliminarily in the field. The setup consisted of hardware for automatic positioning of the laser, instrumentation, data acquisition, and excitation of the rail structure. Computer software was used to command the laser movements and acquire and store data. Analysis and recovery of $T_0$ was subsequently run on a mainframe computer using a Fortran 77 program.

## 5.2 Hardware

The same laser positioning hardware was used for both laboratory and field-testing. The laser positioning system consisted of a Compumotor Zeta 83-93 motor driving a stage on an 8 ft (2.44 m) long Parker HLE-60 scan rail. Two smaller Compumotor HV-233 motors provided vertical and offset movement of the laser on a Parker 802-5470B platform.

A Ramsey SG550 audio generator generated an excitation waveform that was amplified by a Crown DC-300A-2 stereo amplifier. A Labworks 12.5 lbf (56 N) electromagnetic shaker was used to vibrate the rail at a constant frequency. A 6.25-amp bus fuse protected the shaker from excessive current. A Shurite model 8505 ammeter was used to monitor the current to the shaker and to aid the operator in adjusting the shaker power. A household box fan provided cooling for the amplifier.

Initially a magnet was used to fix the shaker rod to the rail. Later it was realized that more energy could be driven into the rail by clamping the shaker to the rail. A clamp was built by modifying a deep 3 in (7.62 cm) C-clamp.

A Polytec PDV100 portable digital vibrometer was used to scan the response at discrete points along the rail based on the heterodyne interferometer principle and the Doppler effect (Guilloteau, 2000). Focusing the laser prior to each scan and maintaining a constant distance from the rail enhanced the laser signal quality. The offset distance from the rail also had to be changed when vertical movements were made; thus, three-axis motion was required for taking quality data.

Three Compumotor Zeta-6104 microstepping drives were daisy-chained and operated via RS-232C serial port communications. The system was addressed so drive 0 controlled motions along the longitudinal axis (z), drive 1 controlled vertical motions (y), and drive 2 controlled offset motions (x) of the laser (Figure 5.1).

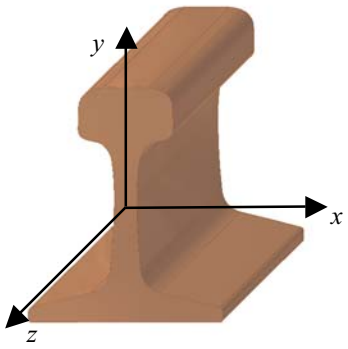


**Figure 5.1 Definition of Rail Scan Axes**

Four PCB Piezotronics 353B33 ICP accelerometers with model 080A27 magnetic bases monitored the baseline vibration of the rail. The accelerometers were powered by a model 482A04 power supply and 10 ft (3.05 m) long model 003A10 microdot cables were used to connect the two. A thermocouple was used to measure and monitor the rail temperature during the test and to take an ambient air temperature reading. A National Instruments BNC-2110 shielded connector block with signal-labeled BNC connectors bundled the signals and a single 12-bit National Instruments DAQCard-6062E in an IBM ThinkPad PC was used for the acquisition and digitization of the waveforms detected by the laser vibrometer and the accelerometers. A National Instruments LabVIEW 6.1 virtual instrument (VI) was written to command data acquisition as well as laser motion via the ThinkPad's serial port.

## 5.3 Loading Jig

A loading jig was built to compress short segments of rail up to 100 kips. The jig was designed to accommodate rails of different sizes and wear patterns. The jig permitted repeatable laboratory tests on compressed rail at various load levels (Chapter 8) and complementary tests on circular rods in tension (Chapter 7).

Four steel plates formed the bulkheads, A, B, C, and D, of the loading jig. Bulkheads A, B, and D were cut from 2 in (5.08 cm) steel plate (Figure 5.2). Bulkhead C was cut from 1.5 in (3.81 cm) steel plate. All bulkheads were 16 in (40.64 cm) square and had clearance fits for 1.75 in (4.45 cm) diameter steel rods at each corner. Nuts on the ends of the rods contained the load during load application; nuts on bulkhead B locked the load into the loading frame for testing.

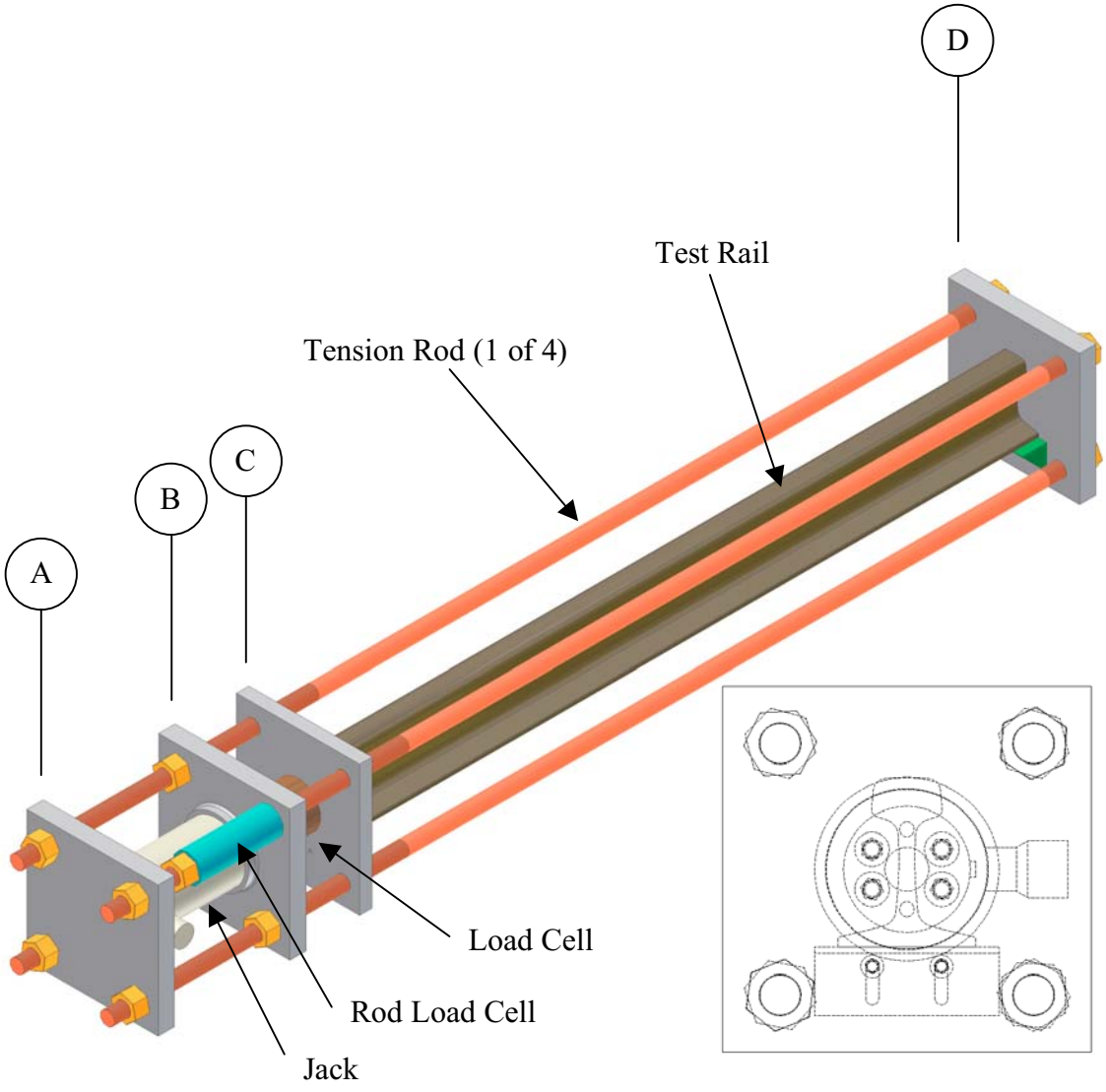


**Figure 5.2 Loading Rig**

An Enerpac RC-1006 hydraulic jack between A and B applied the longitudinal force in the rail via a hand pump. A Lebow 3156 load cell between B and C was used to measure the longitudinal force in the rail. Sacrificial aluminum shims 0.0625 in (1.58 mm) thick were used between the faces of the load cell and the bulkheads B and C.

L3x3x¼ (inch units) steel angles 8 in (20.32 cm) long were used to support the rail on bulkheads C and D. The angles were slotted so their heights could be adjusted to accommodate different size rail. Lead sheets were used between the surface of the rail cross-section and the vertical wall of the support to prevent slipping and to ensure homogeneous end support conditions.

A hollow cylindrical load cell was used between A and B to measure the tensile load in one of the circular rods for the rod study (Chapter 7). The load cell outputs were wired to a strain gauge conditioner that connected to one of the inputs on the BNC-2110 shielded connector block.

## 5.4 Software

National Instruments LabVIEW software version 6.1 was used for data acquisition and preliminary signal processing. Two separate VIs were used in the scanning process. In addition, Compumotor's Motion Architect software was used in the initial configuration of the laser platform.

Compumotor's Motion Architect is a Windows-based software tool for 6000 series controllers. Although it has the capability to generate commented setup code and create, edit and execute motion control programs, for the purposes of this project it was

only used to adjust the starting position of the motors prior to beginning a test. LabVIEW VI serial communications were used to automatically position the laser once a scan was initiated.

Two LabVIEW VIs were used for testing. Because the technique depends on a high signal-to-noise ratio, the rail driving frequency is ideally chosen at or near a resonant frequency. A VI was used to acquire the resonant frequencies prior to the test by taking a 10 second record of laser and accelerometer responses to a large amplitude excitation. A Fourier transform of the recorded data to the frequency domain enabled the operator to identify the resonant peaks on the VI front panel.

Another VI was used to begin data collection after setting the driving frequency at or near a resonant frequency. The VI was structured to allow for full automation of the testing procedure. The first layer initialized commands to properly address the motors and set acceleration and velocity parameters. A second layer compiled a set of scanning positions necessary to conduct the test based on user inputs. Finally, a third layer collected data and then commanded movements of the laser through the serial port. The lock-in technique described by Damljanovic (2003) was used in the VI to filter out the effect of signal noise.

### 5.5 Testing Procedure

Conducting a test was a three-step process. First the test setup was configured and the test specimen prepared. Next, the data were acquired. Finally, the data were analyzed to recover the load and ultimately to determine $T_0$.

### 5.5.1 Laboratory Setup and Preparation

The first step in configuring a test involved setting and recording the load. The hydraulic jack was used to set the desired load in the compression jig while the load cell and the readout generated by the GetLoad.VI was monitored. The nuts on the tension rods on the outboard side of bulkhead B were then tightened and the jack pressure released. Then the actual load was recorded.

The scan platform and laser assembly were positioned near the rail at the preferred offset distance for the laser (Chapter 6.3). The accelerometers were magnetically fixed to the rail and the shaker was clamped to the rail. Once the appropriate power and signal cable connections were made LabVIEW software was opened on the ThinkPad PC and the test initiated.

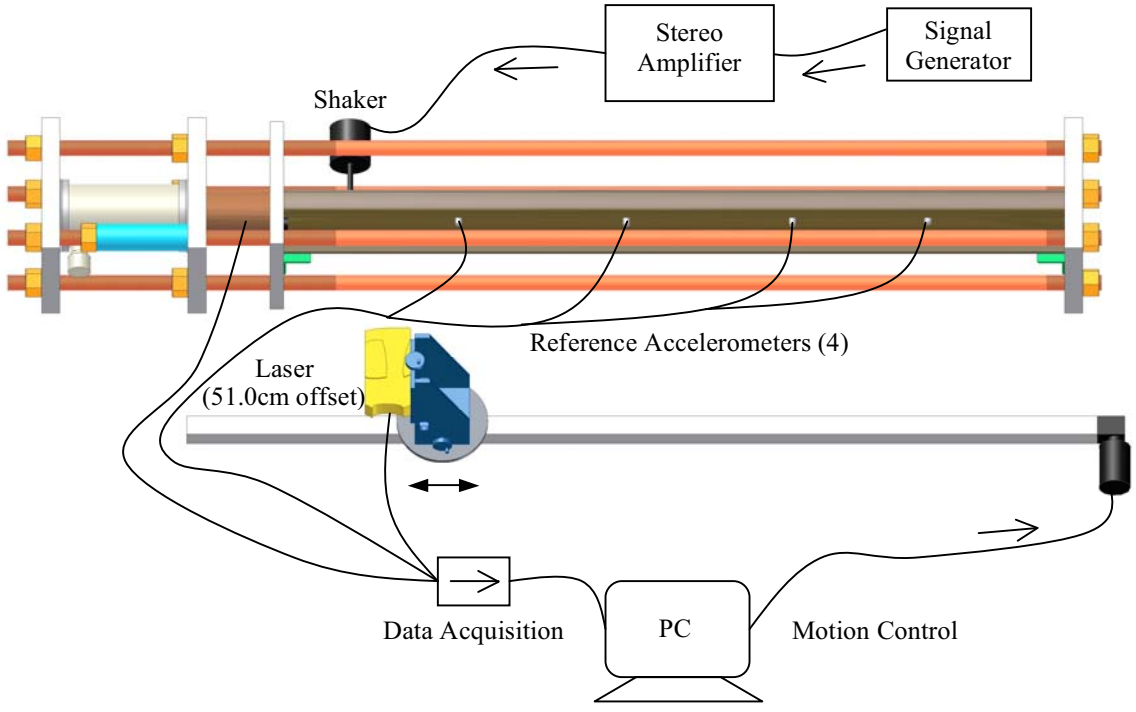


**Figure 5.3 Laboratory Test Setup**

The GetResonantFrequencies.VI was used to determine the resonant frequencies. The program was started and the specimen was struck laterally with a non-metallic object, typically a rubber mallet, to excite its modes of vibration. The representation of the specimen's response in the frequency domain helped to suggest the preferred driving frequencies. The driving frequency was then set in the audio generator and the amplifier turned up until the current being supplied to the shaker approached 6 amps. Next, the VI was opened to begin acquiring data.

### 5.5.2 Data Acquisition

Two VIs were written for data acquisition, one for a circular rod in tension (Chapter 7) and another for laboratory and field tests on rail in both tension and compression (Chapters 8 and 9). The appropriate VI was selected based on the type of test. The scan spacing and number of scan points and the driving frequency were inputted on the VI front panel. Executing the VI began the data collection.

The actual position of the laser, the real and imaginary parts of the four accelerometer signals, the real and imaginary parts of the filtered vibrometer signal, and the temperature were recorded at each scan point. The time and frequency domains of each instrument were displayed on the VI's front panel. The peak heights of each device's response were also displayed and the ratio between two accelerometer peak heights was plotted. Finally, the transfer function between the laser vibrometer and one of the accelerometers (ACC1) was plotted so the operator could estimate the quality and smoothness of the waveform (Figure 5.4).

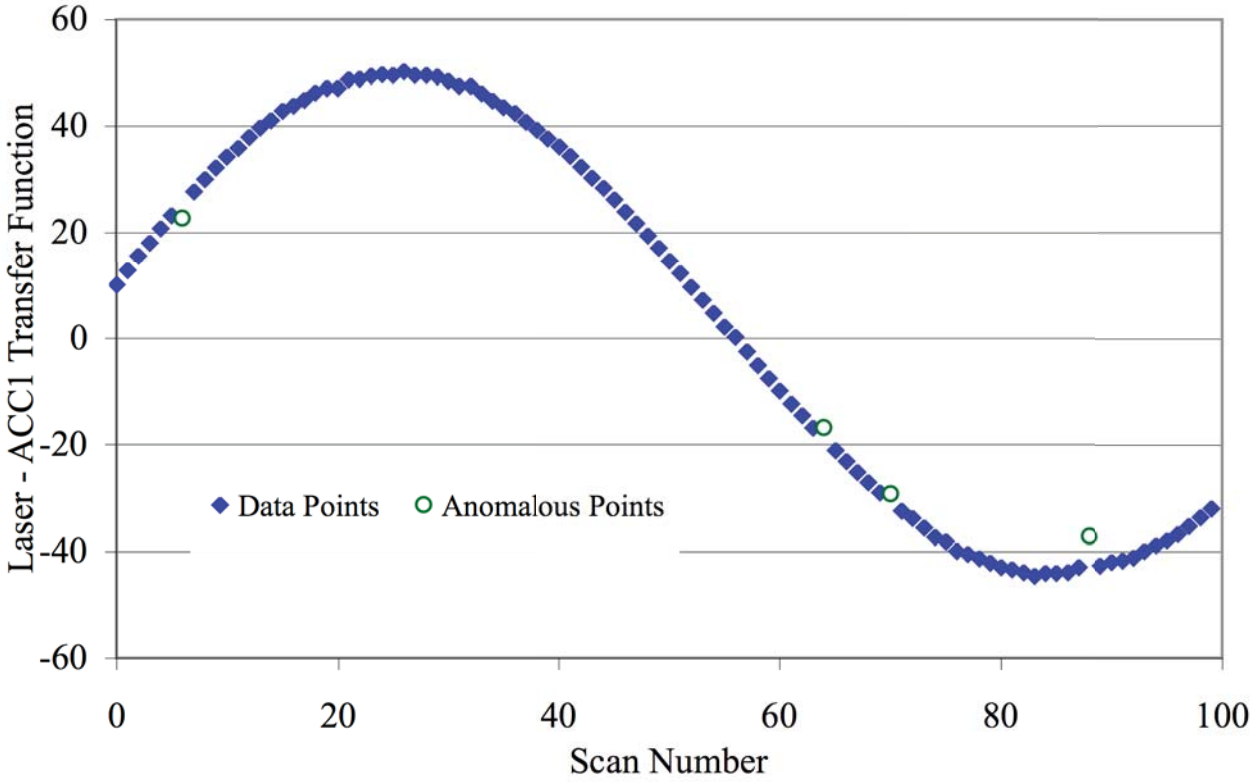


**Figure 5.4 Real Part of Transfer Function**

| Nominal Position (cm) | Encoder Steps (2000steps/cm) | LASER Real | LASER Imag | ACC1 Real | ACC1 Imag | ACC2 Real | ACC2 Imag | ACC3 Real | ACC3 Imag | ACC4 Real | ACC4 Imag | Rail Temp |
|---|---|---|---|---|---|---|---|---|---|---|---|---|
| 0 | 2 | 289.24 | -211.27 | 122.95 | -150.07 | -36.01 | 44.81 | 35.46 | 9.81 | 79.10 | -94.94 | 71.31 |
| 2 | 3986 | -83.30 | -373.24 | -88.91 | -172.25 | 26.87 | 50.80 | 18.22 | -24.85 | -55.71 | -110.27 | 71.34 |
| 4 | 7991 | -93.92 | -396.38 | -91.78 | -170.75 | 27.68 | 50.33 | 21.01 | -25.72 | -57.57 | -109.31 | 71.32 |
| 6 | 11999 | 408.05 | 138.38 | 193.29 | 12.34 | -57.35 | -3.07 | 11.37 | 34.20 | 123.01 | 8.82 | 71.29 |
| ⋮ | ⋮ | ⋮ | ⋮ | ⋮ | ⋮ | ⋮ | ⋮ | ⋮ | ⋮ | ⋮ | ⋮ | ⋮ |
| 200 | 400520 | 82.00 | -446.10 | -16.29 | -193.09 | 5.41 | 57.17 | 33.02 | -17.25 | -9.41 | -123.13 | 71.31 |

**Table 5.1 Raw Scan Data**

The data were saved into a text file of the format shown in Table 5.1. Real and Imag represent the cosine integral part of the waveform and the sine integral part of the waveform, respectively. The resultant data sets are small, in the range of 50kB.

### 5.5.3 Analysis Procedure

The approach used in these experiments was to conduct the analysis after a complete data set was collected. Ultimately, however, the analysis could be incorporated into the same process that acquires the data.

The analysis is run using a Fortran 77 program. It was assumed that the state of the rail vibration drifts in an n-dimensional tangent space, and that the state could be monitored by n accelerometers in different places or with different orientations. Thus the coefficient of any of the waves in the rail is an initially unknown linear combination of the signals from the accelerometers. The coefficients in this linear combination are treated as parameters to be fit by linear regression.

The program fits to the data using a least square residual process. The program also automatically eliminates data points that are more than 2.5 standard deviations from the fit (anomalous points as shown in Figure 5.4) and calculates a best-fit estimate of the wavenumber. A plot of the residual with the anomalous points eliminated from the fit is shown in Figure 5.5.

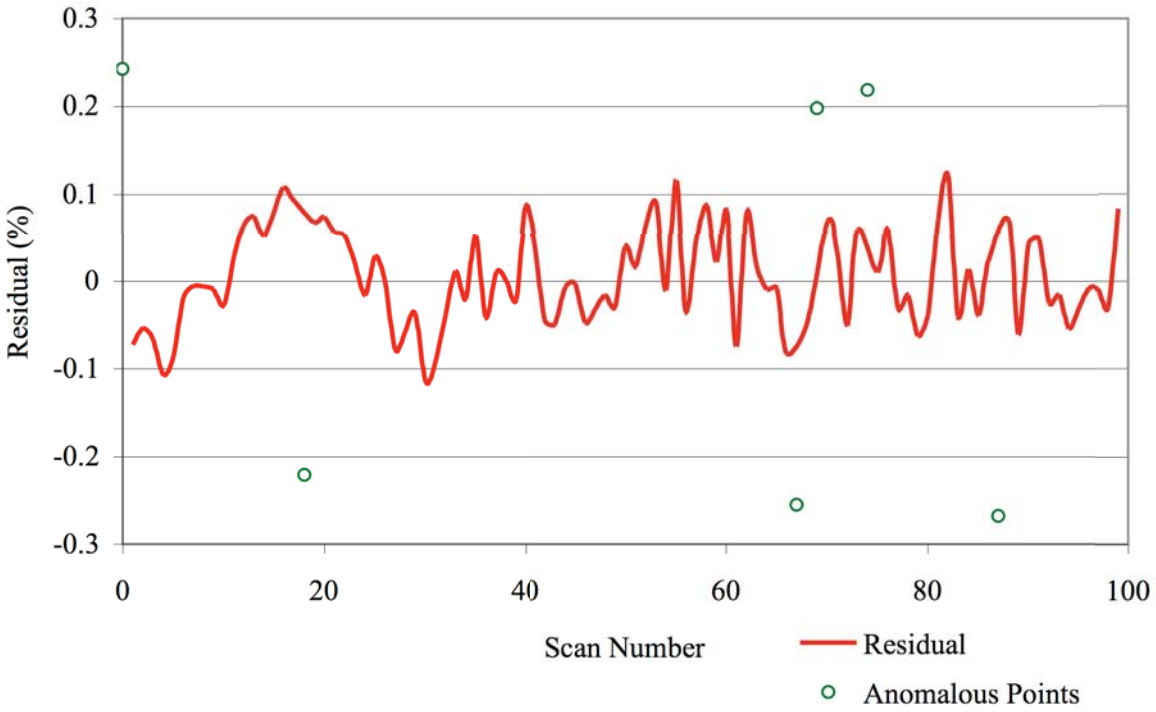


**Figure 5.5 Residual of Fitting Process**

Once at least two values of *k* are recovered from the analysis a plot similar to Figure 5.6 is generated and the value of the intercept ($\frac{S}{\rho A}$) allows extraction of the load as discussed in Chapter 4.

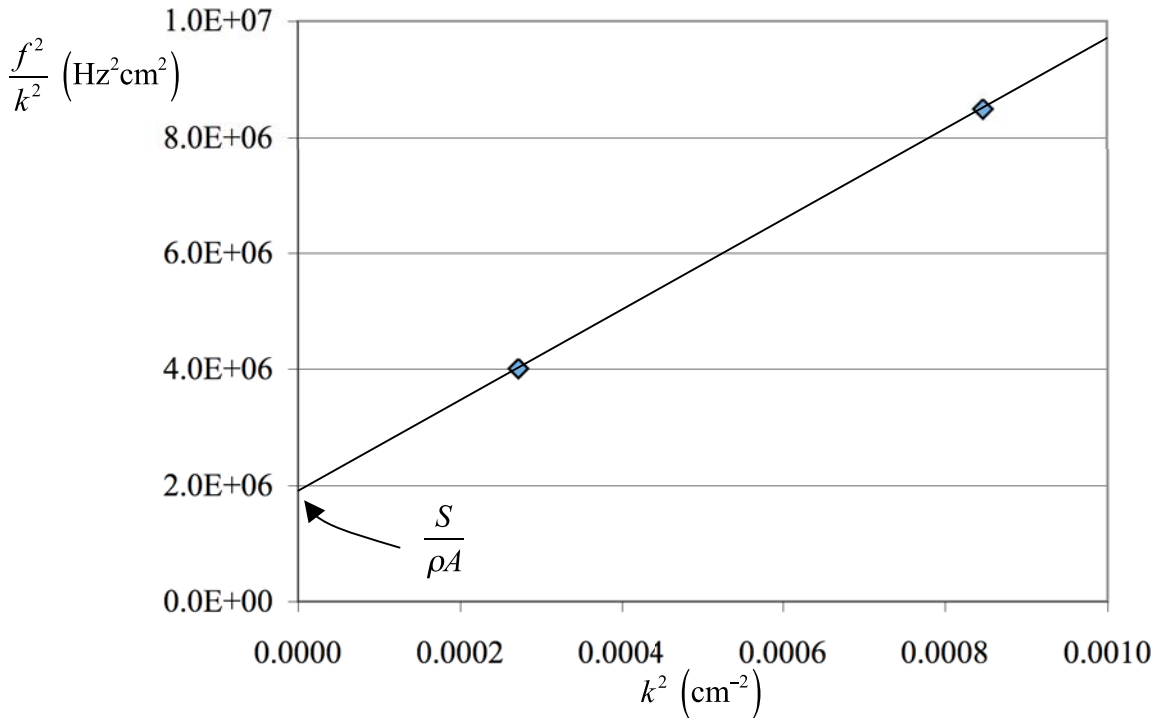


**Figure 5.6 Analysis Results for Two Frequencies**

## 5.6 Conclusions

An efficient and straightforward testing protocol was developed. An operator with little knowledge of the theoretical basis for the method can conduct a test using this technique. Refinement of the process by consolidating steps, for example, the data collection and the analysis phases, would accelerate the overall time required for a test.

# CHAPTER 6

# TECHNICAL CHALLENGES

## 6.1 Introduction

Several conditions must be met in order for the two-frequency approach to accurately estimate $T_0$. The vibration modes on the rail must be stable, the laser must have a high-quality signal, and the scan platform must be free of vibrations. In both laboratory and field, attention to these conditions is essential for quality data and accurate results.

## 6.2 Stability of Modes

The two-frequency approach is based on the Euler-Bernoulli effect of longitudinal load on the vibration of the rail. The technique involves analyzing the wavelengths of standing vibration modes and therefore requires that the modes remain stable throughout the duration of the scan.

Damljanovic (2003) determined that nonlinearities in the supports disrupted mode stability during her laboratory tests. In the research described here additional mechanisms of vibration instability were identified by monitoring the ratios of vibration between several points on the rail during laboratory and field tests. Changes in

temperature that change the state of longitudinal force in the rail altered the shape of the vibration modes (Chapter 9.2.1). In the laboratory, lead sheets were used between the surface of the rail cross-section and the vertical wall of the support to prevent slipping. Load relaxation was observed after compressing the rail to high levels of load as the lead sheets deformed plastically. In the field, vibration of the rail would also cause running, as shaking energy would liberate longitudinal forces locked-in by adjacent rail anchors and fasteners.

In the laboratory, I found that the load would slowly decline for approximately five minutes and remain constant thereafter. In the field I found that striking the rail would release locked-in longitudinal forces (Chapter 9.4.1.1). When testing in the field, I developed ways to control the effect of temperature changes on the state of longitudinal force in the rail by clamping and/or increasing the toe load on the rail (Chapter 9.4.1). To date, however, no way has been found to eliminate the contamination of vibration modes from shocks caused by such things as trains passing on an adjacent track or vehicles driving over the rail at a nearby grade crossing. The use of multiple reference accelerometers was designed to correct for this, as well as the unexplained drift. They are all just drifts as far as the experiment is concerned.

### 6.3 Quality of Laser Signal

The Polytec portable digital vibrometer model PDV100 specifies a group of offset distances as a result of the laser wavelength (Table 6.1). These preferred offset distances

improve the signal quality and therefore the data quality; therefore, it is important to set the offset properly before data collection begins.

| Offset Distance (cm) |
|---|
| 9.6 |
| 23.4 |
| 37.2 |
| 51.0 |
| 64.8 |
| 78.6 |
| 92.4 |
| 106.2 |
| 120.0 |
| 133.8 |

**Table 6.1 Preferred Laser Offset Distances**

In addition to maintaining the constant beam length, the signal quality was enhanced by focusing the laser prior to each scan. In order to minimize beam scattering at the surface and thus improve the vibrometer signal-to-noise ratio, the rail surface to be scanned was cleaned with a wire brush to remove rust and mill scale. In laboratory experiments I also determined that a flat-white paint could be used to slightly improve the vibrometer signal-to-noise ratio thereby reducing the number of anomalous points. This practice was not adopted in the field because it was decided that the benefit of painting the rail did not justify the time needed to do so.

## 6.4 Vibrations in the Scan Platform

The laser vibrometer measured the vibration of a point on the surface of the rail. In order to obtain accurate data it is important that the laser and scan platform are stable

with respect to the rail. Vibrations in the scan platform can contaminate the data by adding, if the scan platform vibration is out of phase with the rail, or subtracting, if the scan platform vibration is in phase with the rail, to the vibrometer signal.

A study on a short track panel was conducted to measure vibration in ties and on different locations on the rail to determine the best way to support the scan rail in the field (Chapter 8.3). Field tests on jointed rail confirmed that a field prototype that was supported on the ties would have the least contamination from vibration (Chapter 9.2). A possible approach not tried in this research would be to monitor the vibration in the laser with an additional accelerometer and subtract its signal from the laser signal.

## 6.5 Conclusions

Several conditions must be met in order for the two-frequency approach to provide accurate estimates of $T_0$. The rail vibration modes must remain stable and can be controlled by allowing the structure to relax in the laboratory and by liberating locked-in longitudinal forces in the field. Structural drifts can be handled by using multiple accelerometers that capture and subtract the changes in the fitting process. The laser signal quality can be improved by setting the proper offset distance and focus. Vibrations in the scan platform have been avoided by developing a prototype apparatus that takes advantage of low vibrations in the ties. Challenges due to adjacent traffic and operations typical of everyday railroading persist.

# CHAPTER 7

# TEST OF THEORY

## 7.1 Introduction

A study on a circular rod in tension was conducted to test the theoretical basis for the two-frequency approach. The compression jig that was developed for loading rail shapes in the laboratory permitted complementary tests of the circular rods in tension (Chapter 5.3). To ensure objectivity in the analysis the data collection and the analysis were two separate phases of the test. The person conducting the analysis was not the person who acquired the data and the actual loads in each test were not revealed to the analyst until after the analysis was completed.

## 7.2 Laboratory Setup

One of the four tension rods on the loading jig (Figure 5.2) was the test specimen. The rod was checked at its quarter-points using digital calipers for out of roundness and changes in profile. A load cell was placed between bulkheads A and B on the rod. The laser vibrometer was used to make one scan of the rod about its centroid (Figure 7.1).

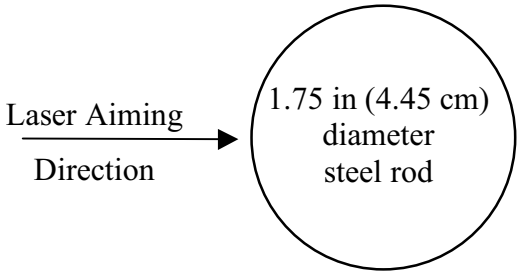


**Figure 7.1. Laser Aiming Direction**

## 7.3 Testing Procedure

The load was set on the rod using the hydraulic jack. Each tension rod carried approximately one-fourth of the compressive load in the frame so the operator set the compressive load approximately four-times the desired load in the rod. The accelerometers were magnetically fixed to the rod and the laser aimed at the centroid of the rod. The laser was offset from the rod by 51.0 cm, one of the preferred distances (Table 6.1), and the scan platform was operated automatically along the rod.

The GetResonantFrequencies.VI was used to identify excitation frequencies with a high signal to noise ratio. At least two frequencies were used; more frequencies were used when possible to ascertain if the data points were collinear. When points were not collinear, those that would fit closer to a slope of $r_g^2 c_{bar}^2$ were used. For a 1.75 in (4.45 cm) steel rod, the radius of gyration, $r_g$, in bending can be calculated,

$$r_g = \frac{d}{4} = \frac{4.45}{4} = 1.11 \text{ cm} \qquad (7.1)$$

Damljanovic (2003) measured $c_{bar}$ to be 505000 cm/s, therefore, in the proper units,

$$c_{bar}^2 r_g^2 = \left(505000\right)^2 \left(1.11\right)^2 \left(\frac{1}{2\pi}\right)^2 = 8.10\text{e}9 \text{ Hz}^2\text{cm}^4 \qquad (7.2)$$

The method does not require that $c_{bar}^2 r_g^2$ be known prior to testing, but knowing the value verifies the slope of the line and helps estimate the accuracy of the data.

The compression jig permitted a scan range of approximately 220 cm on the tension rod. Scans were typically 80 data points recorded at 2 cm to avoid the 30 cm nearest each bulkhead where vibrations are partially contaminated by evanescent modes not included in the data analysis. In an effort to stabilize the vibration modes, the leveling compound HydroCal was set under each of the bulkheads (Figure 7.2).

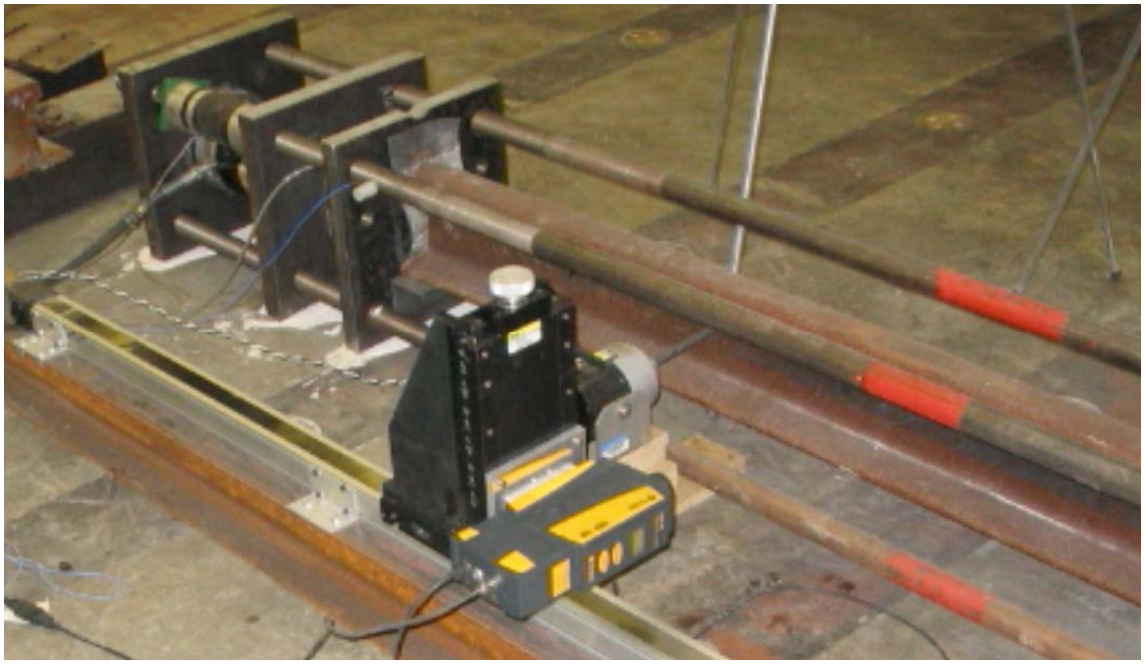

**Figure 7.2 Rod Study Setup**

The recovered load was compared to the actual load before the next data set was collected. This process revealed deficiencies in the data collection and analysis technique and suggested improvements for subsequent data sets.

## 7.4 Results

A total of twenty-three load cases were collected (Table 7.1). Load cases A, B, and C used only one reference accelerometer; therefore, small trends in the data caused by structural shifts were not manageable during the analysis process. These trends resulted in obviously erroneous wavenumbers for load cases A and C. All subsequent load cases used four reference accelerometers and the analysis code was able to tolerate nearly 20% trends in the ratio between any two accelerometers.

The analysis of load case L had a high residual caused by an unusually large number of anomalies in the data. These were probably caused by dust on the surface of the rod. The rod was periodically wiped clean throughout the remainder of the tests, which improved the quality of the laser signal.

| Load Case | Actual Load (kips) | Recovered Load (kips) | Error (kips) |
|---|---|---|---|
| A | 14.90 | | |
| B | 4.15 | 4.00 | -0.15 |
| C | 10.45 | | |
| D | 10.64 | 9.48 | -1.16 |
| E | 18.85 | 13.43 | -5.42 |
| F | 21.60 | 14.78 | -6.82 |
| G | 1.88 | 3.00 | 1.12 |
| H | 23.19 | 29.80 | 6.61 |
| I | 8.10 | 10.01 | 1.91 |
| J | 6.32 | 6.42 | 0.10 |
| K | 12.61 | 12.43 | -0.18 |
| L | 16.29 | | |
| M | 17.84 | 21.00 | 3.16 |
| N | 15.23 | 19.40 | 4.17 |
| O | 20.94 | 20.70 | -0.24 |
| P | 22.94 | 24.40 | 1.46 |
| Q | 24.71 | 24.80 | 0.09 |
| R | 27.21 | 19.70 | -7.51 |
| S | 14.30 | 12.80 | -1.50 |
| T | 17.65 | 20.90 | 3.25 |
| U | 20.15 | 19.80 | -0.35 |
| V | 23.56 | 24.06 | 0.50 |
| W | 26.06 | 25.44 | -0.62 |

**Table 7.1 Rod Study Results**

The accuracy of the fit was judged by comparing the slope of the fit and the exact slope, 8.10e9 $Hz^2cm^4$ (Equation 7.2). Load cases with slopes that nearly matched the exact value were generally better fits. Load case I had a slope of 8.16e9 $Hz^2cm^4$ (Figure 7.3), which is less than a 1% deviation from the exact slope.

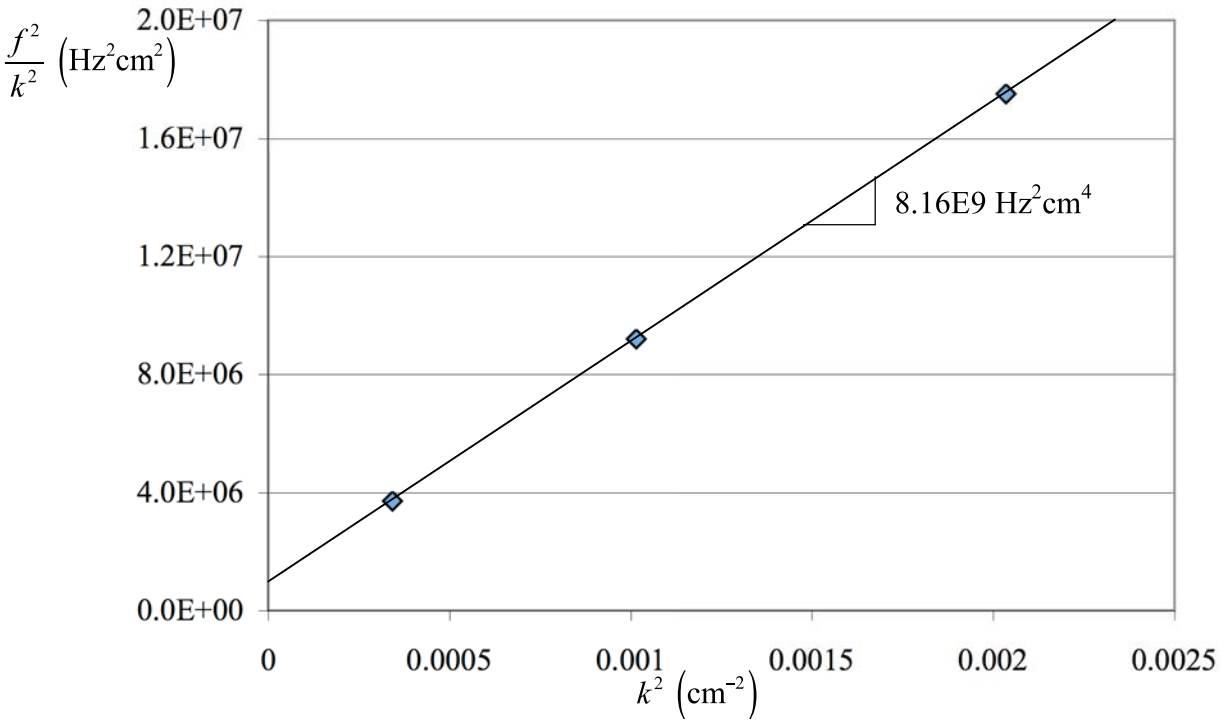


**Figure 7.3 Load Case I Results**

There was some indication of more scatter at loads greater than 15 kips (Figure 7.4). Increasing the shaker force by clamping the shaker to the rail provided a higher signal-to-noise ratio and therefore a higher quality signal in the laser. The final four load cases, T-W, were excited by a clamped shaker and are identified separately in Figure 7.4.

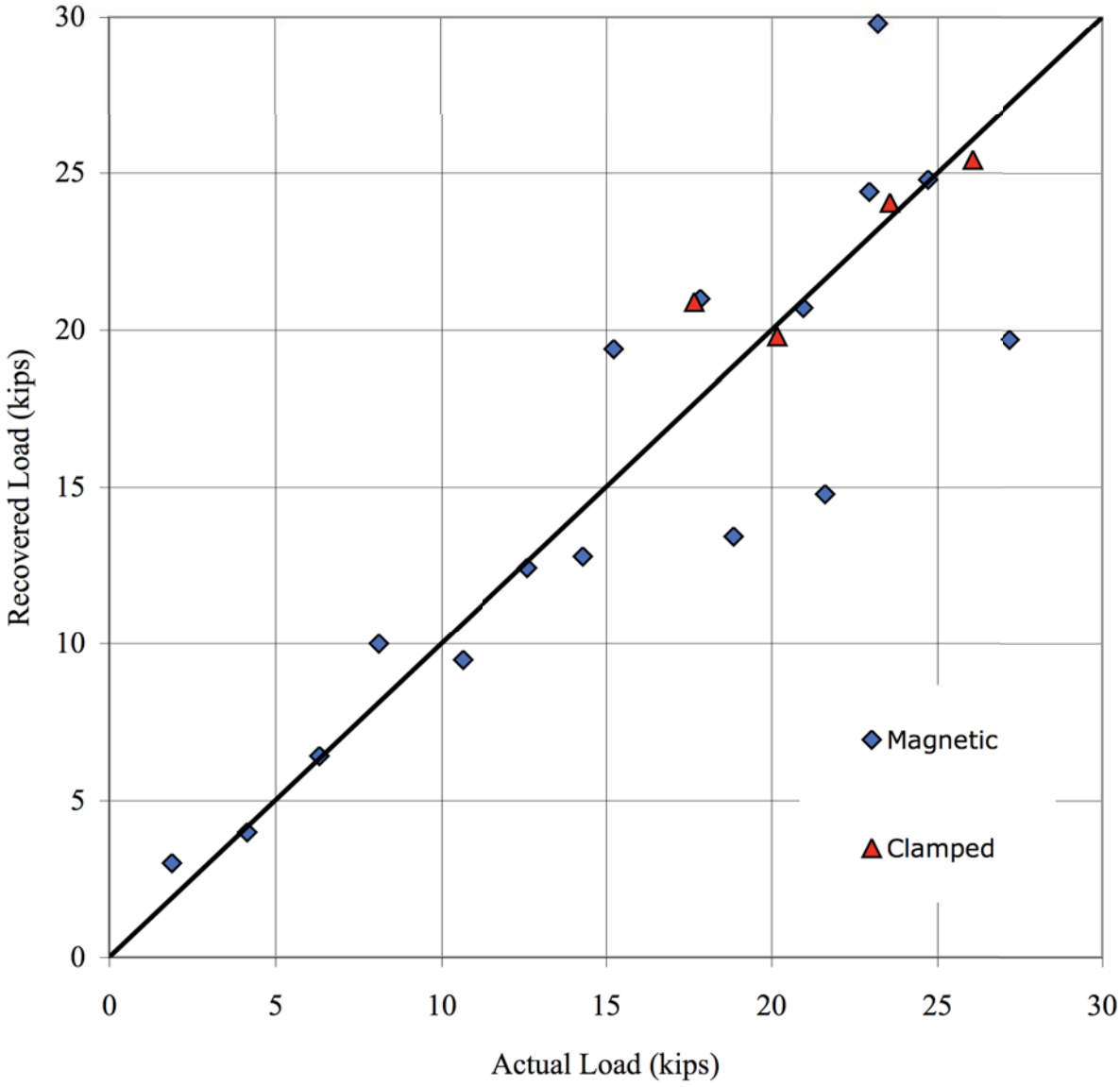


**Figure 7.4 Plot of Rod Study Results**

The clamped data points, T-W, had error less than 4 kips for all points and appear to have conformed better. Overall, the largest error was 7.5 kips. The average error was -0.2 kips, suggesting that the scatter in the data was unbiased. The standard deviation (SD) was 3.4 kips and for clamped load cases the SD was 1.8 kips.

## 7.5 Conclusions

The results of the tests on a circular rod in tension are consistent with predictions based on the two-frequency approach. The final load cases using a clamped shaker and four reference accelerometers had a SD less than 2 kips. The next step was to apply the method on rail.

# CHAPTER 8

# LABORATORY STUDIES ON RAIL

## 8.1 Introduction

The laboratory test of circular rods in tension showed that the two-frequency method could be used to calculate longitudinal load with reasonable accuracy under controlled conditions. The next step was to use the method to assess the longitudinal force in rail. The vertical asymmetry of rail makes the analysis more complicated because the torsional modes must be subtracted in the analysis to recover the lateral bending wavenumber. Laboratory studies were conducted on an unworn (new) and a worn 136RE rail in the compression jig at loads between 0 kips and 100 kips. Data were collected for twenty-four load cases.

## 8.2 Compression Jig

Data were collected at three heights (Figure 8.1) and at two or more frequencies for each load case. Two of the heights were located on the web of the rail, and one was located on the head (Figure 8.1). Multiple heights were necessary to subtract the effect of the torsional modes. The clamped shaker was used to excite the rail.

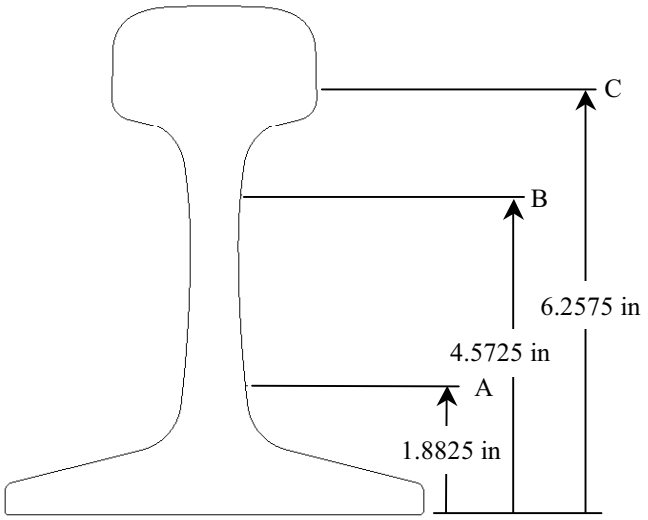


**Figure 8.1 Scan Heights**

### 8.2.1 Unworn Rail

An 87 in (221 cm) long section of unworn 136RE was tested in the compression jig. The scans were completed at 1.8825, 4.5725, and 6.2575 in (4.7816, 11.6142, 15.8941 cm) above the base of the rail (Figure 8.1). Each scan contained 83 data points recorded at 2 cm intervals; the total scan length was 1.66 m (5.45 ft). All load cases used four magnetically fixed reference accelerometers on the web of the rail, two just outside the scanned portion of the rail, and two in the scanned portion.

Thirteen load cases were collected on the unworn rail section (Table 8.1). I determined that the data acquisition format in the VI used in the first test was erroneous, so load case A could not be analyzed and it was not included in the final data analysis. The VI was reprogrammed and run for twelve additional load cases. During load cases I and J the power amplifier overheated and tripped during the scan as a result of dust. Consequently, these cases were also omitted from the analysis. The amplifier was

cleaned with compressed air, which solved the problem and the remaining tests were run successfully.

| Load Case | Actual Load (kips) | Recovered Load (kips) | Difference (kips) | Difference (°F) |
|---|---|---|---|---|
| A | 80.12 | | | |
| B | 89.40 | 74.00 | -15.40 | -6.1 |
| C | 54.38 | 80.30 | 25.92 | 10.3 |
| D | 18.64 | 29.73 | 11.09 | 4.4 |
| E | 42.30 | 55.70 | 13.40 | 5.3 |
| F | 10.68 | 2.00 | -8.68 | -3.4 |
| G | 5.59 | 7.00 | 1.41 | 0.6 |
| H | 96.41 | 70.00 | -26.41 | -10.4 |
| I | 96.83 | | | |
| J | 74.67 | | | |
| K | 62.94 | 77.10 | 14.16 | 5.6 |
| L | 74.05 | 49.87 | -24.18 | -9.6 |
| M | 31.05 | 48.17 | 17.12 | 6.8 |

**Table 8.1 Unworn 136RE Rail Study Results**

Overall the recovered load was within 11°F of the actual load. The average neutral temperature error was 0.3°F, which suggests that the error was unbiased. The SD was 7.3°F.

On average, each height took 15 minutes to scan. Since data were collected at three heights and at two frequencies, the total test time was approximately 1 hour 30 minutes for each load case.

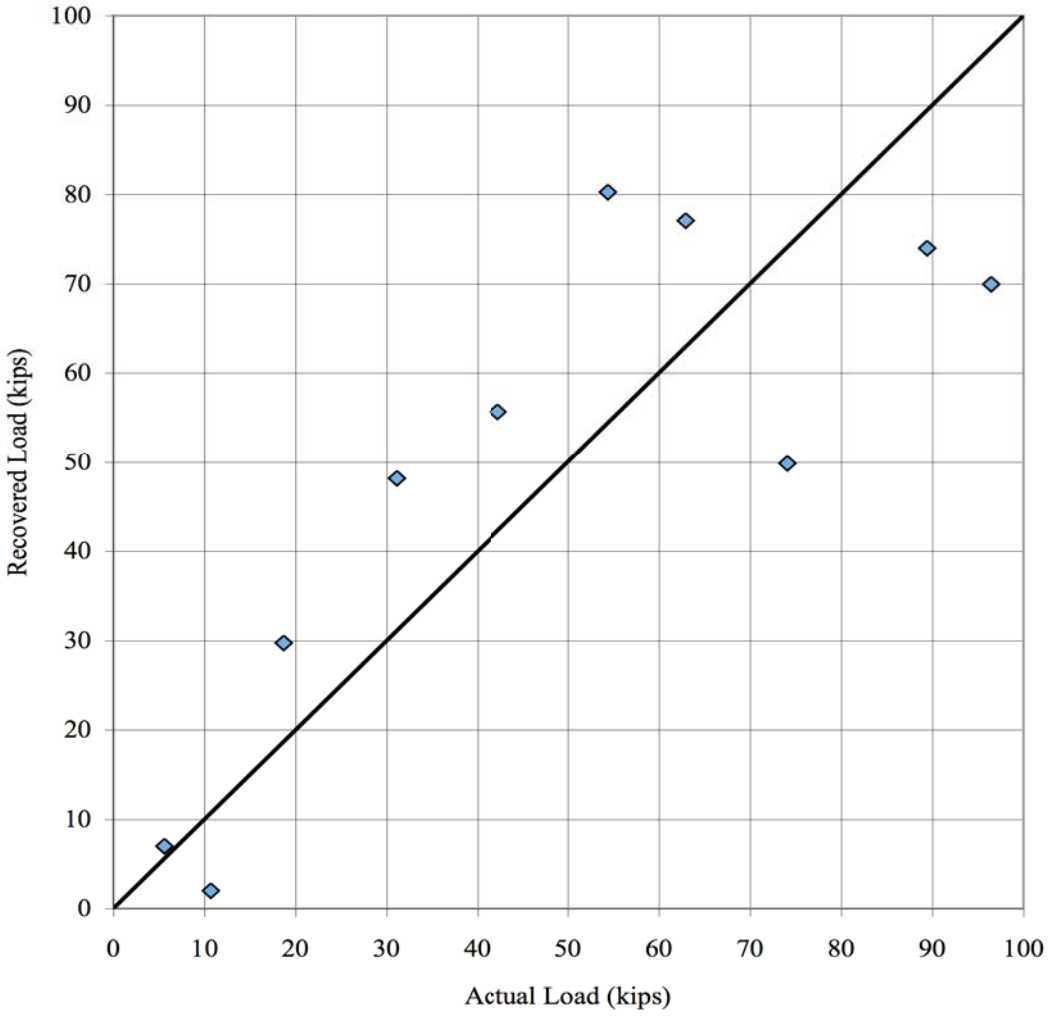


**Figure 8.2 Plot of Unworn 136RE Rail Study Results**

### 8.2.2 Worn Rail Shapes

A study using the same protocol was conducted on worn 136RE rail in the compression jig. The scans were completed at the same heights on the rail. The scans included the same number of data points and reference accelerometers as the unworn rail study.

Eleven load cases were collected (Table 8.2). The average neutral temperature error was -2.6°F and the SD was 13.0°F.

| Load Case | Actual Load (kips) | Recovered Load (kips) | Difference (kips) | Difference (°F) |
|---|---|---|---|---|
| A | 23.85 | 57.00 | 33.15 | 13.8 |
| B | 57.30 | 8.82 | -48.48 | -20.2 |
| C | 80.03 | 82.00 | 1.97 | 0.8 |
| D | 9.81 | 40.00 | 30.19 | 12.6 |
| E | 20.90 | 11.60 | -9.30 | -3.9 |
| F | 38.20 | 65.00 | 26.80 | 11.2 |
| G | 50.95 | 57.00 | 6.05 | 2.5 |
| H | 71.30 | 67.00 | -4.30 | -1.8 |
| I | 93.52 | 74.00 | -19.52 | -8.1 |
| J | 82.15 | 17.40 | -64.75 | -26.9 |
| K | 33.70 | 12.00 | -21.70 | -9.0 |

**Table 8.2 Worn 136RE Rail Study Results**

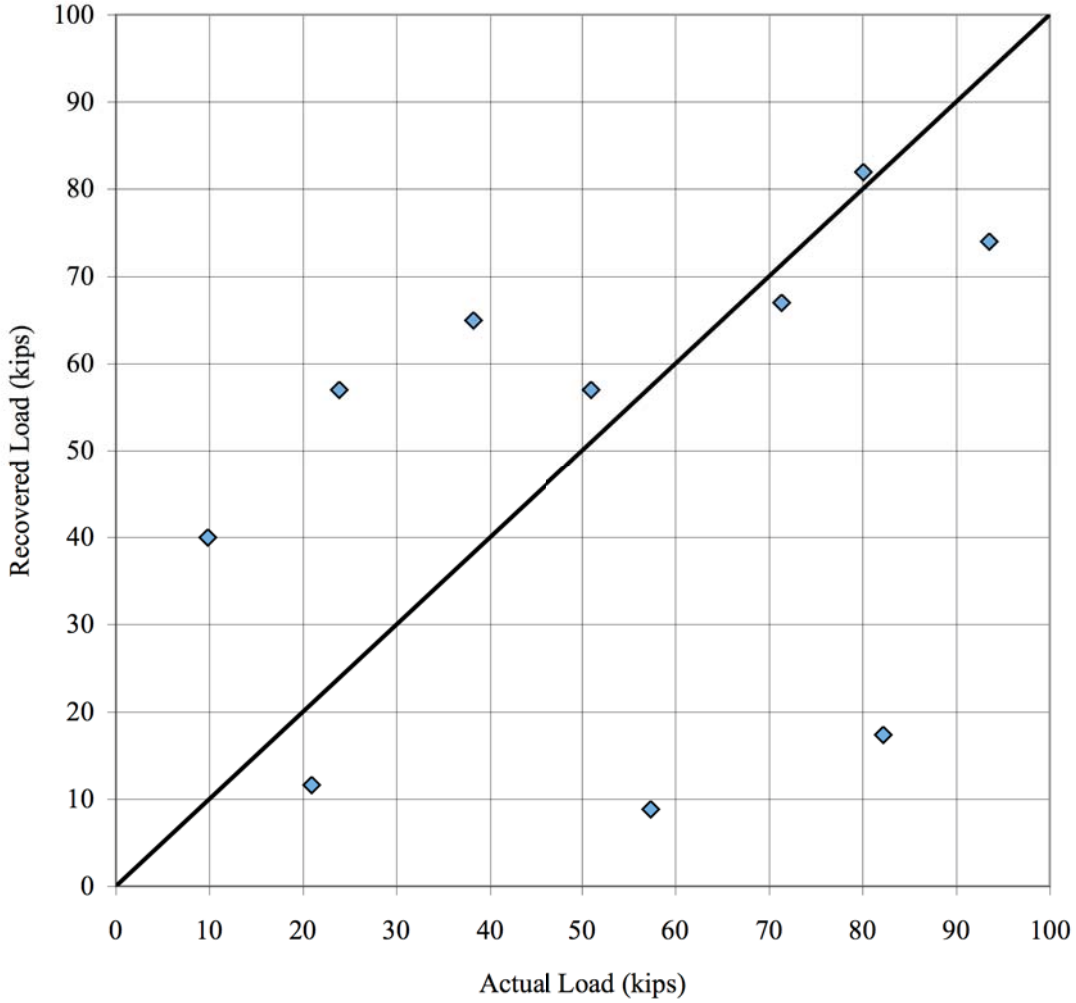


**Figure 8.3 Plot of Worn 136RE Rail Study Results**

Considerable scatter was noted in the worn rail study results (Figure 8.3). The torsional wave speed predicted by Damljanovic (2003) on *unworn* 136RE rail was used in this study after investigating the effect of wear on the torsional wave speed (Appendix) and concluding that wear has some, but only a little, effect. It was found, however, in those cases where there were three frequencies available to analyze, that the highest frequency cases had vibrations dominated by torsional waves (amplitudes 3 to 10 times greater than the bending wave). If the high cases were dropped, and a two-point plot

done, the inferred load was much closer to the actual. For example, load case B infers a load of 36 kips compression if the high frequency (194.60 Hz) data set is dropped. It is thus tentatively concluded that the torsional wave speed taken from the FEM code for unworn rail, and thus only approximate for worn rail, is the source of the error. Similarly it may be that the mode shape presumed (i.e., how much tilt there is in the bending mode and how much mean displacement there is in the torsional wave) could also be in error for worn rail. These are questions that should be addressed in future investigations.

### 8.3 Track Panel

A study of track structure vibrations was conducted in the laboratory on a 15 ft (4.6 m) track panel provided by the CN Railway. The panel had timber ties and was placed on the laboratory floor without ballast. Tests were conducted to facilitate development of a practical prototype unit to efficiently conduct tests using the technique in the field.

A magnetic-based accelerometer was magnetically fixed to the head of galvanized roofing nails that were set into several locations on the panel and the peak vibrations recorded. The peak vibrations were also recorded at points along the head of the rail.

The vibrations were three-times stronger on the head of the rail than on the ties. Difficulty in isolating the vibrations in the track from the field prototype showed that a design that was supported on the ties would be necessary (Chapter 9).

## 8.4 Conclusions

Studies of unworn and worn 136RE rail were tested in the laboratory. The SD of the results on unworn 136RE rail was 7.3°F and the SD of the results on worn 136RE rail was 13.0°F. The analysis of the tests on worn rail may have suffered from inaccurate predictions of torsional wave speed. Tests on a track panel influenced the design of a field prototype that was used to apply the technique in the field.

# CHAPTER 9

# FIELD STUDIES

## 9.1 Introduction

Field tests were conducted on jointed rail to investigate the distribution of vibrations in the track structure. A practical, robust, field-operable prototype was designed and constructed based on the results. Additional studies of the stability of vibration modes were completed on jointed rail and CWR. Finally, the protoype was used to estimate $T_0$ in CWR.

## 9.2 Vibration Tests on Jointed Rail

Tests were conducted on 90 lb/yd jointed rail with timber ties to investigate technical challenges (Chapter 6) and ways to mitigate them in the field. The study of vibrations in the track structure (Chapter 8.3) was revisited in the field to finalize the prototype design. The site used for the study was the Andersons grain distribution center west of Champaign, Illinois. This site was well suited for this phase of the field-testing because it had minimal rail traffic and easy vehicular access.

### 9.2.1 Stability of Modes

One magnetic-based accelerometer was fixed to the web of the rail and recorded the vibration at a point on the gauge side of the rail as the shaker excited the rail from the field side at a frequency of 80.00 Hz (Figure 9.1). Rail temperature was simultaneously recorded and the drifts in the temperature and the peak accelerometer response were plotted (Figure 9.2).

**Figure 9.1 Accelerometer Monitoring Rail Vibrations**

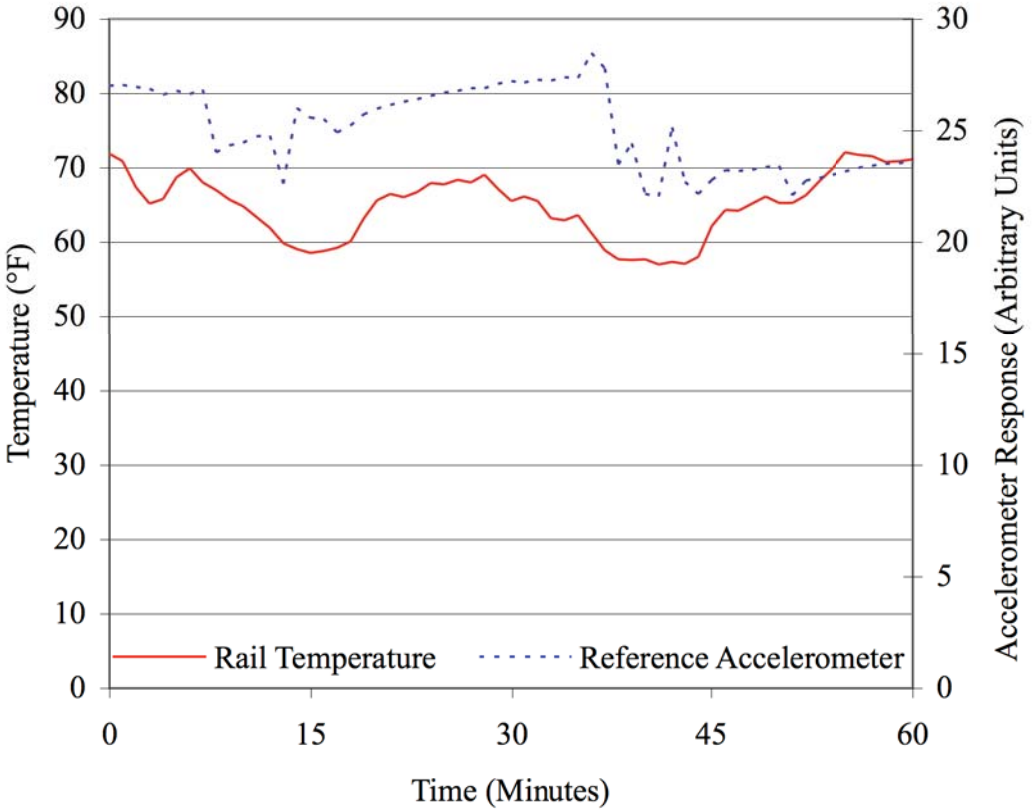


**Figure 9.2 Rail Temperature and Accelerometer Response**

Sky conditions were partly-cloudy the day of the tests and ambient air temperature was approximately 50°F. The rail responded to periods of direct sunlight and periods of cloud-cover with rapid temperature changes.

The general similarity between the temperature and reference accelerometer trends suggests that the response of the accelerometer was influenced by changes in rail temperature and corresponding changes in rail longitudinal force. Over the one-hour record the reference accelerometer signal varied by more than 20%. Over the short term (for instance from 0-7 minutes and 17-35 minutes in the record) the accelerometer drifted less, due in part to a more stable rail temperature and presumably a more stable longitudinal force in the rail.

The results highlighted the importance that tests be performed as quickly as possible because, in the field, rapid temperature changes capable of changing the longitudinal force in the rail are possible.

### 9.2.2 Vibrations in the Track Structure

Vibrations in the track structure were studied in the field to provide information that would be used to finalize the prototype design. The objective was to understand the relative vibrations in different parts of the track structure. The rail was left fastened to the ties and the shaker was used to excite the rail at 110.00 Hz. The condition with the rail fastened could be considered a worst case compared to the anticipated actual test conditions when the vibrated rail would be unfastened. Permission to conduct tests on unfastened rail was not given by the track owner, but the test served its purpose of providing information pertinent to the design of the field-testing apparatus.

2 in (5.08 cm) long nails were set halfway into the ties, 12 in (31 cm) on each side of the track centerline. A single magnetic-based accelerometer was used to take sequential measurements of peak vibrations on the 0.25 in (0.64 cm) diameter nail head as well as along the head of the rail (Figure 9.3).

**Figure 9.3 Magnetic-Based Accelerometer Attached to a Nail in Timber Ties**

The peak accelerometer responses at tested locations on the track structure are summarized in Figure 9.4. The peak accelerometer response is a function of the amplitude of vibration in the rail and is dependent on the calibration of the accelerometer. Locations with no measurable vibration have a peak accelerometer response of zero. Although the exact amplitudes of vibration are not presented here, the peak response of the accelerometer is used to identify the relative vibration of the different components of the track structure.

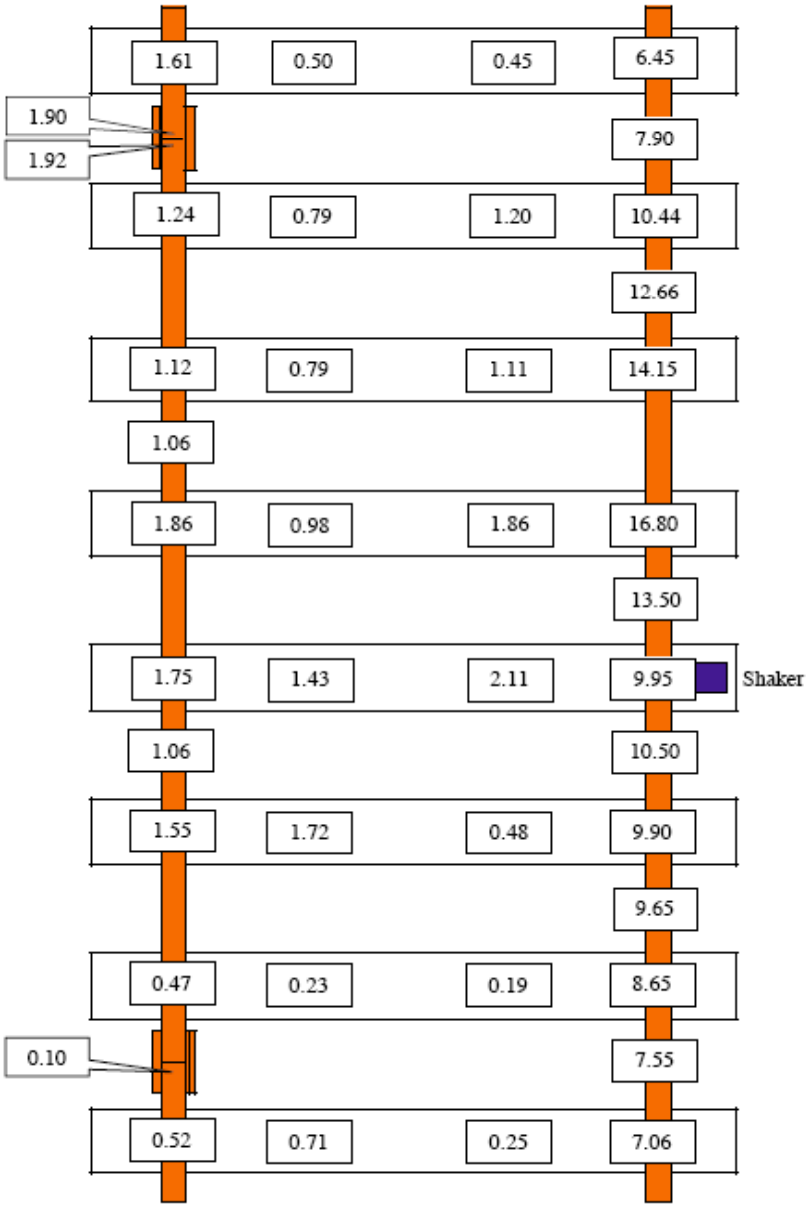


**Figure 9.4 Peak Accelerometer Responses (Arbitrary Units)**

The peak response of the accelerometer was significantly higher on the head of the vibrated rail than on the other rail or on the top of the ties at 110.00 Hz. These results suggested that the field apparatus should be supported on the ties or opposite rail rather than directly on the vibrated rail head.

### 9.3 Field Prototype

A prototype apparatus was designed to adapt the laboratory setup for use in the field. In the initial design the laser scan platform was to be supported by the rails. There were several benefits to this approach; the rail head would aid in the vertical alignment of the laser and the weight of the apparatus would help limit shifting of the rail in the tie plates. However, the results of laboratory tests on a track panel (Chapter 8.3) and field studies of vibrations in the track structure described above, indicated large vibrations along the head of the vibrated rail that would be difficult to isolate from the prototype. Therefore, a design that was supported on the ties was developed instead.

Steel frames with a 28.0 in (71.1 cm) wide footprint supported a steel W6x20 "I"-beam 11 ft (3.35 m) long (Figure 9.5). The scan rail was bolted to the beam and field tests were conducted as in the laboratory, but with the laser in the inverted position. Bolt holes were patterned into the beam 2 in (5.08 cm) on-center that allowed the length between the frames to be adjusted to accommodate different tie spacings. For these tests shims were used under the frames to adjust the laser height with respect to the rail, but ultimately the system needs a fast and easy way to adjust this parameter. A Honda EU2000i generator powered all electrical equipment in the field.

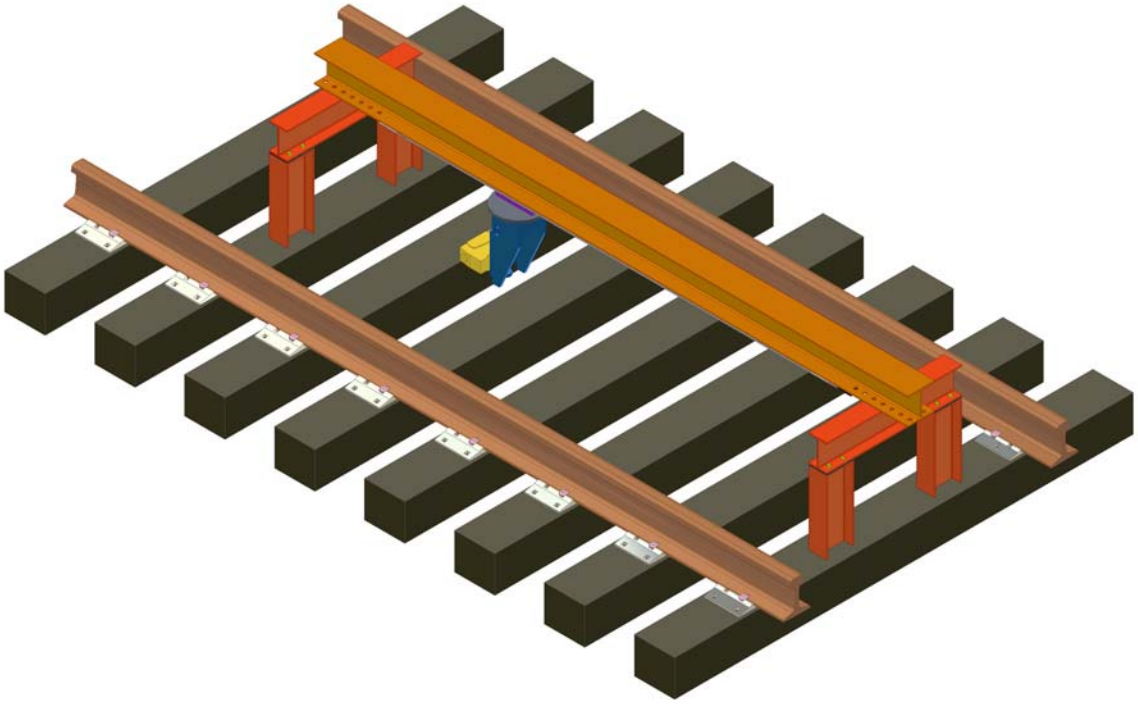

**Figure 9.5 Field Prototype**

Because the prototype design is mounted on the ties midway between the rails it has the capability to scan both rails, although this practice has not been implemented thus far. The track centerline design would allow the laser to swivel and take aim at the other rail or a bidirectional laser could scan both rails simultaneously (Figure 9.6).

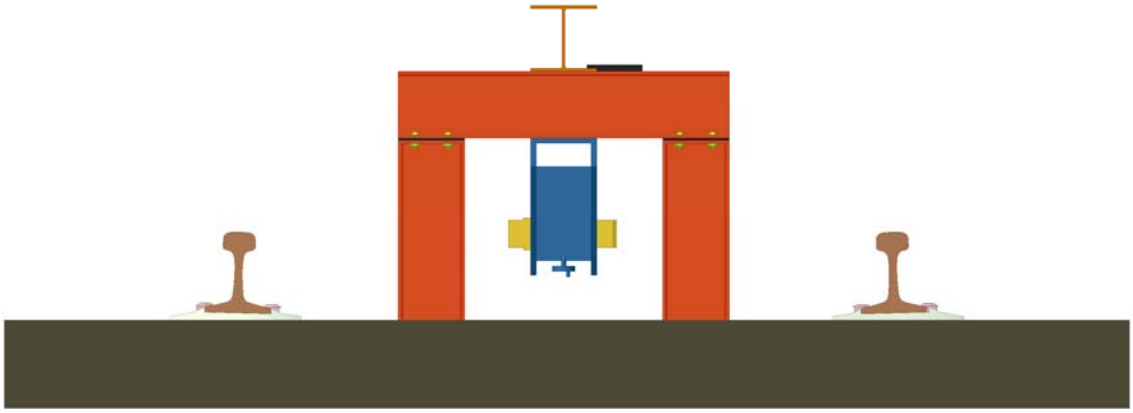

**Figure 9.6 Centerline Prototype Design**

## 9.4 Tests on CWR

The vibration technique was tested in the field on CWR using the prototype. Tests were conducted on track at the Transportation Technology Center (TTC) Facility for Accelerated Service Testing (FAST) near Pueblo, Colorado and on a mainline siding near Rantoul, Illinois on the CN Railway, Chicago subdivision. Both sites were instrumented with strain gauges that enabled continual readings of longitudinal force in the rail.

### 9.4.1 FAST

Studies at FAST on 136RE CWR investigated ways to condition the track in order to minimize drifts of the track structure. Drifts were monitored by collecting peak vibration responses with the laser vibrometer at one point on the rail web and peak vibration responses with an accelerometer (ACC) at another point on the rail web.

#### 9.4.1.1 Timber Tie Track

The rail with timber ties was excited at a constant frequency of 85.50 Hz and the ratio between the laser vibrometer and ACC varied by 5% during the first 5 minutes and then slowly increased for about 10 mintues, and then became relatively constant (Figure 9.7).

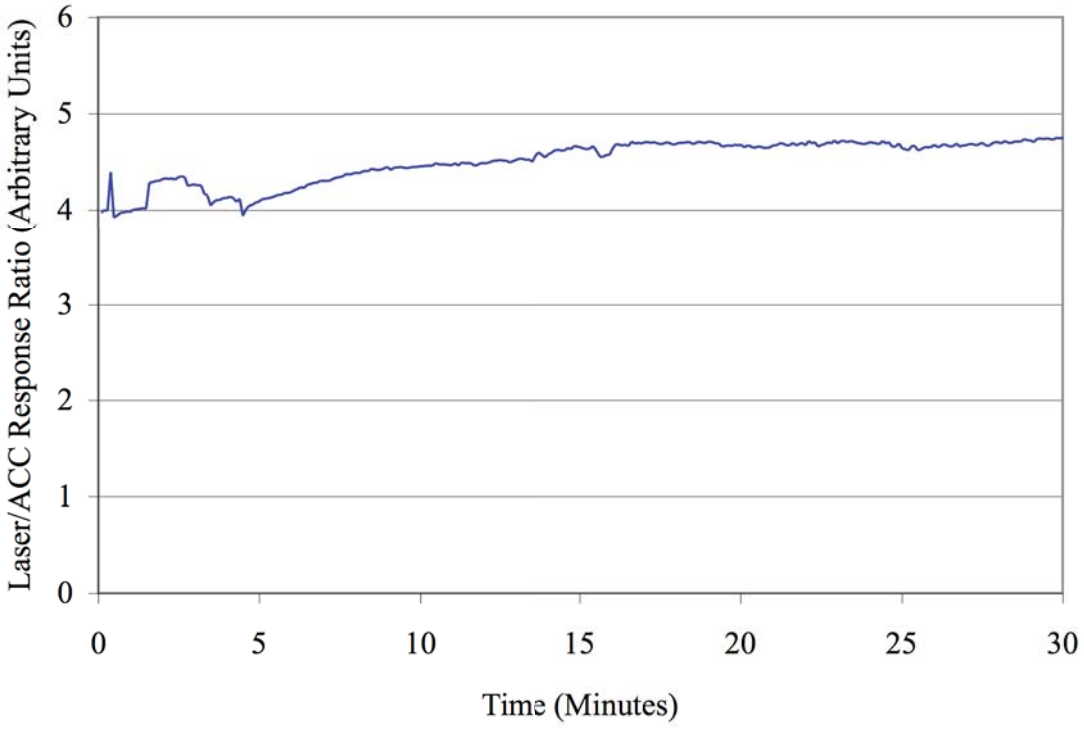


**Figure 9.7 Laser/ACC Response Ratio on Timber Tie Track**

Two ways were evaluated to stabilize the track structure on timber ties. First, a normal load was added to the rail by placing 90 in (229 cm) segments of rail on the rail head at both ends of the scan range (Figure 9.8). The weights helped stabilize the structural drifts in the first 10 minutes, limiting drifts to 2.7% (Figure 9.9).


**Figure 9.8 Rail Segments on Rail Head**

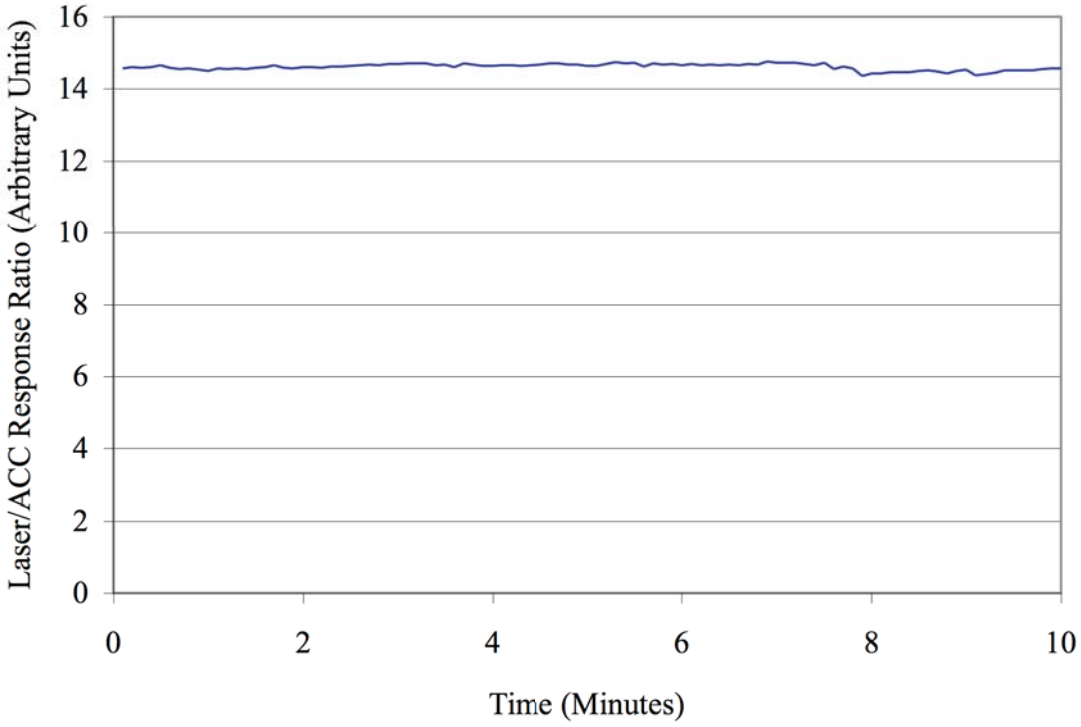


**Figure 9.9 Laser/ACC Response Ratio on Timber Tie Track with Weights**

In the next test steel wedges were driven between the tie plates and the tops of the ties to increase the toe-load on the rail (Figure 9.10) (with weight removed). The wedges had a greater benefit than the rail weights, limiting structural drift to within 1.3% in the first 10 minutes (Figure 9.11).

**Figure 9.10 Steel Wedges Between Tie Plates and Timber Ties**

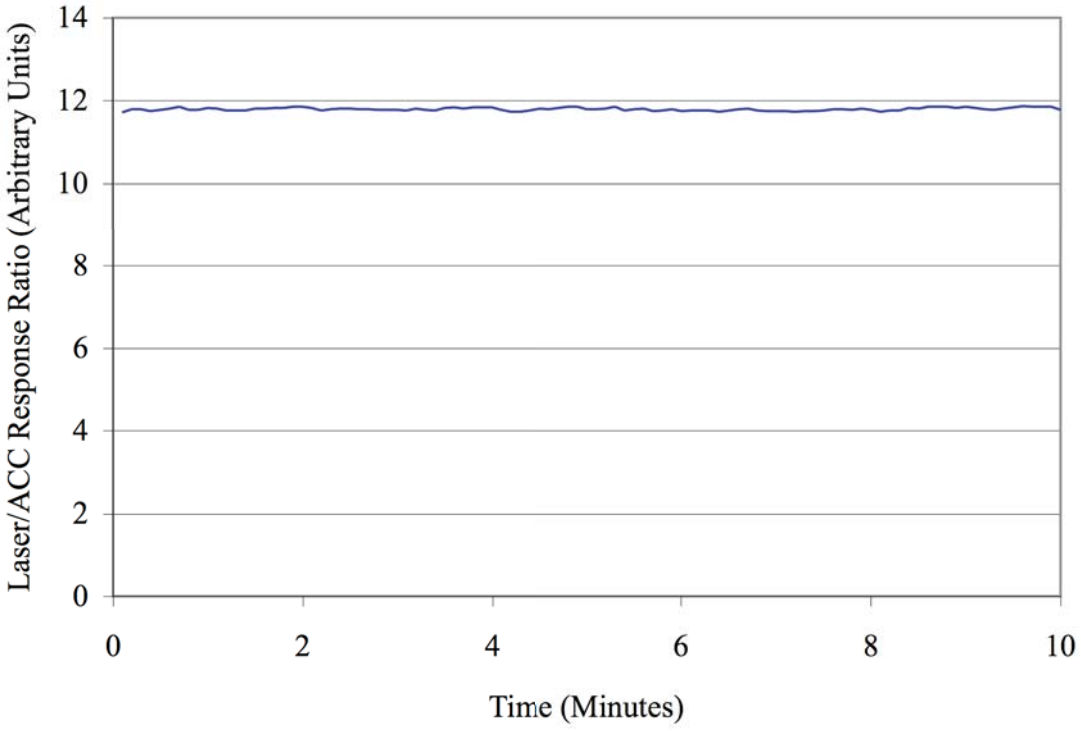


**Figure 9.11 Laser/ACC Response Ratio on Timber Tie Track with Wedges**

### 9.4.1.2 Concrete Tie Track

Concrete ties provided a structure that was much more resistant to drift. Initial studies on concrete ties had 2.5% drifts over 10 minutes when a driving frequency of 49.80 Hz was used (Figure 9.12).

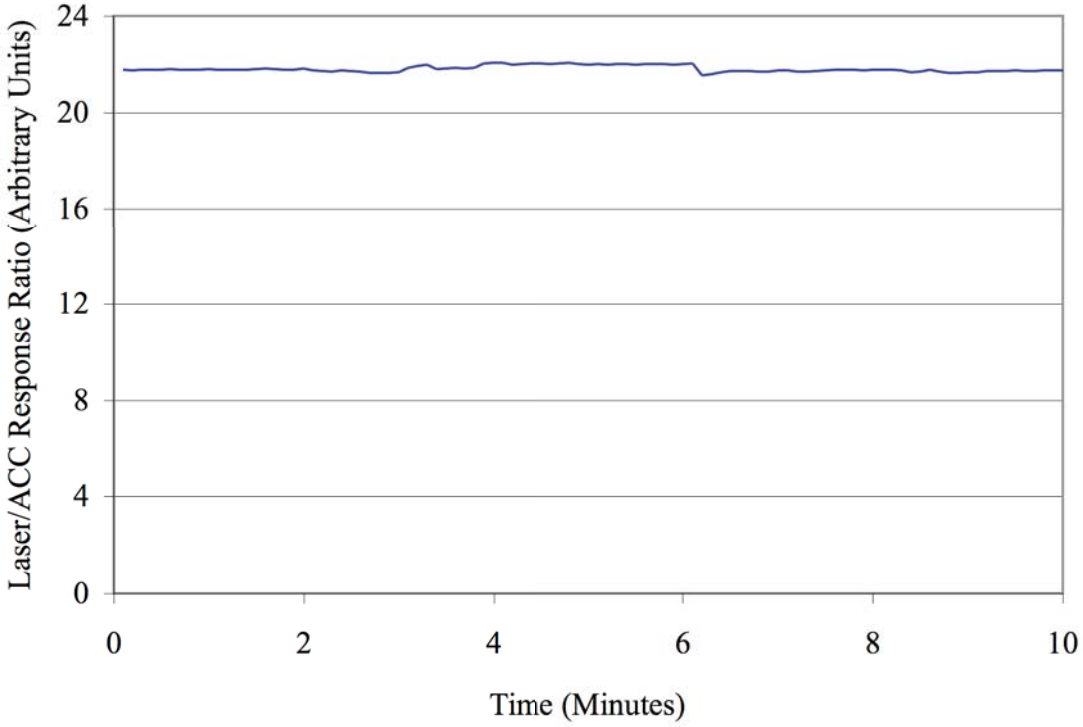


**Figure 9.12 Laser/ACC Response Ratio on Concrete Tie Track**

Track jacks next to the rail fasteners at each end of the scan length were used to increase the toe load on the rail and reduced structural drifts (Figure 9.13). The jacks helped to limit structural drifts to within 2.3% in the first 10 minutes (Figure 9.14).

**Figure 9.13 Track Jacks on Concrete Tie Track**

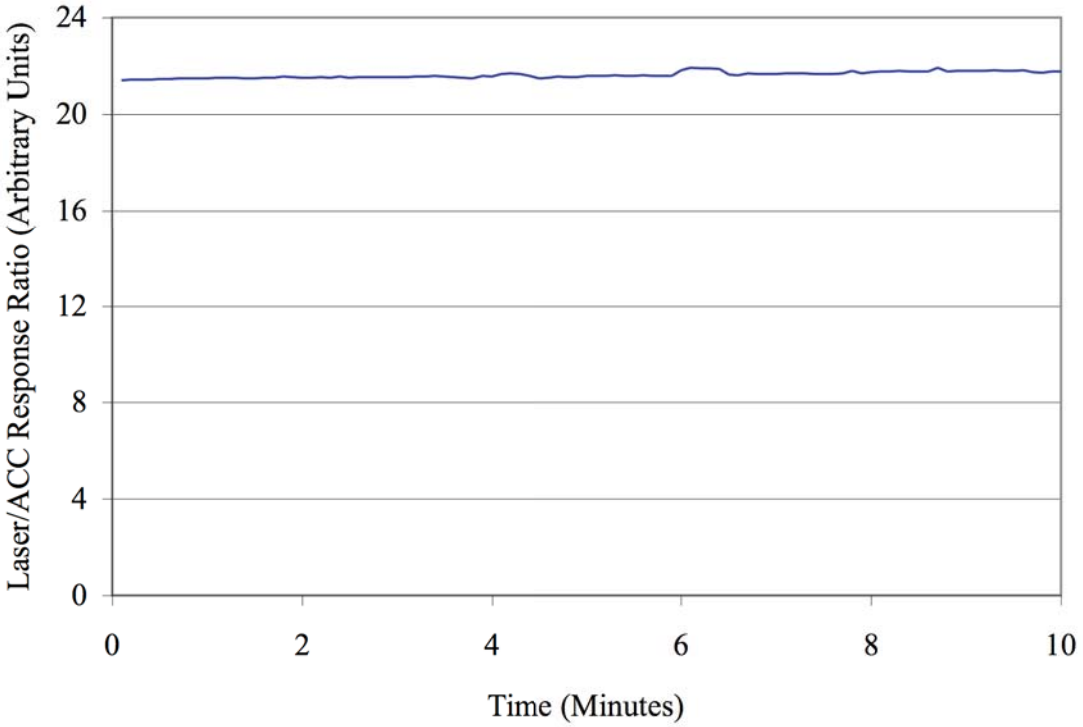


**Figure 9.14 Laser/ACC Response Ratio on Concrete Tie Track with Jacks**

It is possible that the jacks might have the unintended effect of altering the longitudinal force in the rail. This effect and ways to correct for it should be the objects of future studies.

### 9.4.2 CN Siding

Data were collected on a CN Railway mainline siding in Rantoul, Illinois to estimate neutral temperature in 136RE rail. The rail was supported on timber ties nominally spaced every 20 in (51 cm) with cut-spike fasteners. The ambient air temperature was 89°F and the rail temperature was 117°F. The rail neutral temperature was 92°F. The difference between the temperature of the rail and $T_0$ was 25°F, which corresponded to a longitudinal force of approximately 60 kips compression at the time of the test. Neither the force nor the rail temperature was revealed to the data analyst until after the analysis was completed.

The field prototype was supported on the ties (Figure 9.15). Data were collected at three heights (Figure 8.1). Data were collected at four frequencies, 50.00 Hz, 55.00 Hz, 136.00 Hz, and 155.00 Hz.

**Figure 9.15 Field Test Setup on CN Siding**

A wire brush was used to remove rust and mill scale from the surface of the rail prior to testing (Figure 9.16). (The strain gauge installation is also visible in Figure 9.16)

**Figure 9.16 Preparing the Rail Surface**

Fasteners and anchors were removed from the rail over three ties allowing a range of 150 cm for scanning. Four accelerometers were used to monitor the structure during the tests (Figure 9.17). All four were magnetically-fixed to the web of the rail spaced at approximately 50 cm. The clamped shaker was used to vibrate the rail.


**Figure 9.17 Accelerometer and Shaker Setup**

Data acquisition and control was conducted from the laptop setup next to the track in a small flatbed trailer (Figure 9.18). Use of the trailer enabled setup and configuration of the prototype next to the track before permission to be on the track was granted and enabled rapid clearing of the track when testing was completed.

**Figure 9.18 Data Acquisition Setup Next to CN Siding**

High noise signals in the laser vibrometer signal due to solar glare in the laser and a short scan length made the data unable to be analyzed at 50.00 Hz and 55.00 Hz. The two other data points at 136.00 Hz and 155.00 Hz were plotted in Figure 9.19. In this case, $\frac{\omega^2}{k^2}$ versus the FEA prediction of $\frac{\omega^2}{k^2}$ for *unworn* rail were plotted so that the Timoshenko correction could be applied to the data. (The FEA values of $\frac{\omega^2}{k^2}$ are proportional to $k^2$.)

The slope of the fit in Figure 9.19 is 25% lower than it should be for unworn rail (slope of one); which suggests far more wear than was observed on the rail specimen in the field. I am also reluctant to trust these data because the extrapolation to zero recovers an intercept of 26,516. The value of $\rho A$ for unworn 136RE is 67.46 kg/m (136 lb/yd). Considering the light wear in the field rail, I reduced the value of $\rho A$ to 64.50 kg/m (130 lb/yd).

$\rho A$(26,516) = 64.50(26,516) = 1.7 MN = 380 kips (tension)

This recovered load of 380 kips tension is obviously erroneous. Because the data were taken at two relatively high, and not very different frequencies (19.00 Hz difference between the two), the extrapolation to zero was very sensitive to error.

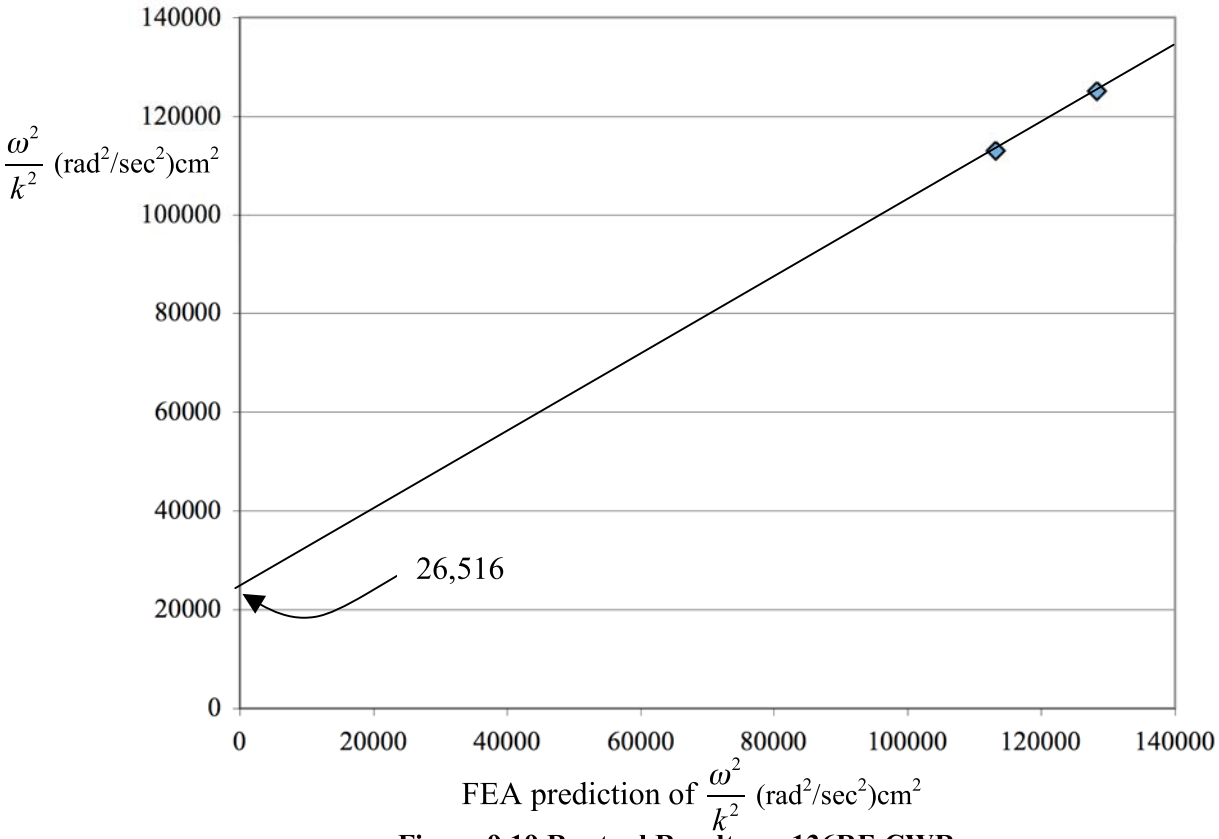


**Figure 9.19 Rantoul Results on 136RE CWR**

Thus I was left with the one frequency method and had to assume that the FEA had intrinsic rigidity that could be sufficiently applicable to this worn 136RE field specimen. If I apply the approach used by Damljanovic (2003) to the 136.00 Hz data I recover a longitudinal force of 20 kips tension. If I apply the approach to the 155.00 Hz data I recover a longitudinal force of 78 kips compression. The actual longitudinal force in the rail was 66 kips compression but the tests results were inconclusive.

The field test would have benefited from the use of a parasol to reduce glare in the laser. Structural stability was adequate and the drifts were tolerable. The use of wedges on the rails was not necessary for the tests primarily because the rail temperature was approximately constant while the data were being collected and, therefore, the longitudinal force in the rail was nearly constant.

## 9.5 Conclusions

Tests were conducted on jointed rail to provide insight regarding the best design for the test apparatus and protocols. The study of vibrations in the track structure was revisited in the field and the results helped to finalize the prototype design.

Vibration tests at FAST developed ways to stabilize the track structure and control structural shifts in the field. On timber ties, both weighting the head of the rail and driving wedges between the tie plates and the ties helped reduce structural shifts. Concrete ties provided more stability to the track structure, and track jacks further reduced structural drifts. If track jacks are to be used as part of a practical field apparatus, then their possible effect on the state of longitudinal force in the rail should be an object of future study.

Ideally, more field-testing of the technique would have been conducted; however, time did not permit this. Still, there are several important findings that will influence the design and execution of future tests. Preliminary tests on CWR in the field suffered from poor laser signal quality at low frequencies. Data at high frequencies were very sensitive to error and recovered an erroneous value of longitudinal force in the rail. The approach used by Damljanovic (2003) was applied to the data but the longitudinal force in the rail was inconclusive. The success of future field studies would profit from use of a parasol over the laser and data collection at lower frequencies.

# CHAPTER 10

# FURTHER WORK

## 10.1 Review

The method of estimation of neutral temperature presented in this thesis has shown varying degrees of accuracy. Laboratory tests on a circular rod in tension provided the most accurate results. Lab studies of a railroad rail were less reliable, particularly on worn rail, because the effects of wear on the torsional wave speed are not yet well understood. The membrane analogy of elasticity was used in an attempt to estimate this effect (Appendix) but the study was applied to only two sets of unworn and worn rail profiles. Additional FEAs on rail profiles with varying degrees of wear would help to quantify this effect.

The next step involves extensive field-testing of the technique on different size rail with varying degrees of wear. Tests should verify the ability of the technique to estimate neutral temperature in rail subjected to a range of tensile and compressive load cases, not just compressive ones as in the laboratory tests conducted thus far.

A review of the accuracy and speed of the technique should be completed to determine ways to further reduce the time needed for the scans and to quantify the cost in accuracy when doing so. Laboratory and preliminary field tests typically used a 2 cm scan spacing between data points, but in the field a longer space between scans could be

used to reduce the data collection time. Unfastening the rail from fewer than the three ties currently used in tests would reduce the preparations to the track structure but would also reduce the portions of vibration modes "visible" in the analysis. Reducing the impact on the track and reducing the time need for a test in this manner, however, would have a similar effect of reducing the accuracy of the technique.

The TTC FAST facility provides an ideal site to conduct a sensitivity analysis of the method and refine the technique for industry adoption. There is relatively unhindered access to track constructed to typical Class I mainline standards. Furthermore, there are equipment and expert personnel available to assist in setting up and executing tests.

### 10.2 Industry Adoption

Ultimately, a satisfactory compromise between the accuracy and speed of the vibration technique needs to be arrived at. Efforts to condition the field to the ideal conditions in the laboratory would certainly demand longer time to conduct a test but would likely be more accurate.

North American railroads struggle to obtain track time for maintenance-related activities but it is possible that rail flaw detection companies could incorporate estimation of $T_0$ into their regular rail flaw detection services. Rail defect detection vehicles (Figure 10.1) are well equipped to power sensitive electronic equipment and their personnel are trained in the operation of such measurement devices (Schmidt, 2005).


**Figure 10.1 High-Rail Rail Flaw Detection Vehicle**

One concept is to tow a neutral temperature measurement apparatus behind a detection vehicle in a manner similar to that illustrated in Figure 10.1. The device would trail the vehicle at a sufficient distance so as not to interfere with other detection activities and so that the vibrations in the rail caused by the engine of the detection vehicle would not interfere with data collection. Mounting the device on a trailer that is supported on the rails, however, requires creative ways of eliminating vibrations from the scan platform, e.g. mounting an accelerometer on the laser to "subtract" the vibrations in the laser from the laser signal.

## 10.3 Conclusions

The vibration technique presented in this thesis has the potential to satisfy the requirements for a nondestructive technique to estimate $T_0$ as specified by Kish and Samavedam (1987) and Weaver and Barkan (2000). The device is portable, measures the absolute value of force in the rail, and is independent of residual stresses. Further research in the laboratory should investigate how adaptable the technology is to different size and wear patterns of rail present in the field. Further studies in the field should determine if the technique is able to achieve the goal of $T_0$ estimation with ±5°F accuracy while being performed within 30 minutes.

# APPENDIX

# EFFECTS OF RAIL PROFILE CHANGES ON TORSIONAL WAVE SPEED

## A.1 Introduction

The two-frequency approach that uses the relationship between two or more driving frequencies and two or more corresponding wavenumbers eliminates the need for finite element analysis of the rail (Chapter 4). Elimination of FEA is important for the technique to become viable in the field because of the variety of rail sizes and possible wear patterns that can occur in the field. Conducting an FEA of these is not practical and unknown wear patterns might make this impossible anyway. During analysis, contributions from the torsional wave must be subtracted from the lateral bending wave; therefore, the effect of wear on torsional wave speeds was investigated.

The effects of rail profile on the speed of the torsional wave were studied on four rail profiles, unworn and worn 136RE and unworn and worn 115RE. The torsional wave speeds were predicted for each of the profiles using the membrane analogy of elasticity and the change in torsional wave speed was investigated for each of the rail sizes.

## A.2 Theory

St. Venant torsion theory assumes that the cross section remains plane and the radii remain straight, an accurate theory only when applied to the case of the circular shaft away from the applied traction (Timoshenko and Goodier, 1970). The membrane analogy is useful for computing torsional rigidity when there is warping of the cross section and inclination of the cross-section planes (Timoshenko and Goodier, 1970). Figure A.1 shows the warping of the cross-sections that takes place when a non-circular shaft is subjected to torsion.

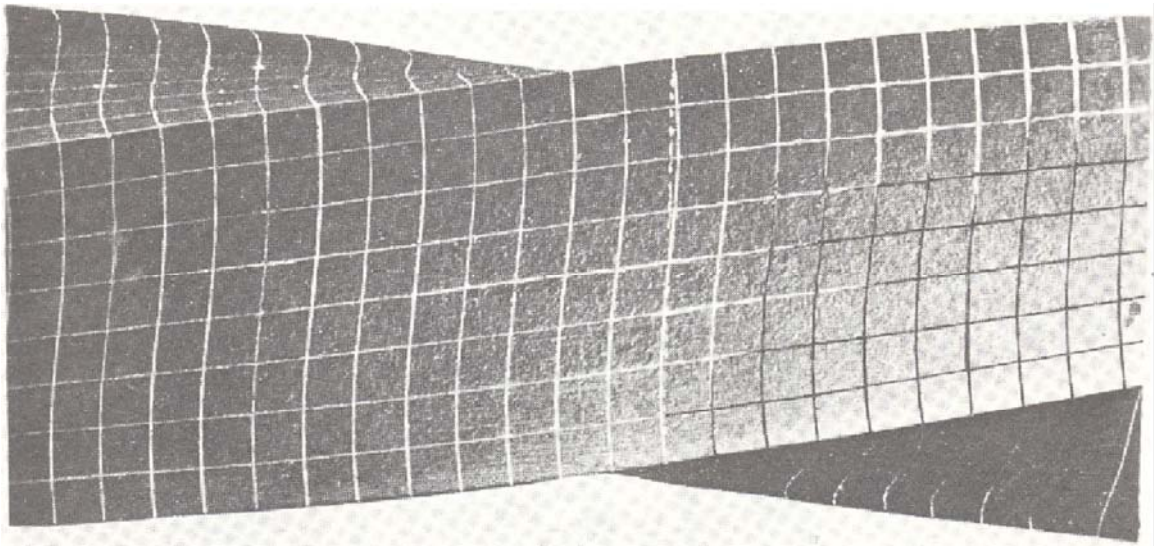

**Figure A.1 Square-Prismatic Shape Subjected to Torsion** *(Timoshenko and Goodier, 1970)*

The out-of-plane warping of the cross-section, expressed as $\psi(x,y)$, is needed to develop the expression for the kinetic energy of the shaft (Graff, 1975). The displacement, *u*, of any point on the cross section can be described by the vector equation (Timoshenko and Goodier, 1970),

$$\vec{u}(x,y) = \theta(z)\hat{k} \times \vec{r} + \theta'(z)\psi\hat{k} \qquad \text{(A.1)}$$

Where $\vec{r}$ is the position vector from the center of mass to a point on the rail cross-section, $\hat{k}$ is a unit longitudinal vector, and $\theta'$ is the twist, or change in angle, $\theta$, per change in length $\left(\theta' = \frac{\partial \theta}{\partial z}\right)$. The expression for the kinetic energy, *KE*, of the system subjected to a torsional wave is,

$$KE = \int \frac{1}{2} \rho \left[ \dot{\theta}^2 r^2 + \dot{\theta}'^2 \psi^2 \right] dx dy dz \tag{A.2}$$

The potential energy, *PE*, of a structure subjected to a torsional deformation is,

$$PE = \int \frac{1}{2} C \theta'^2 dz \tag{A.3}$$

where *C* is the static torsional rigidity of the shaft.

The Lagrangian, *L*, of the system is *KE* less the *PE*,

$$L = \int \left[ \left( \frac{1}{2} \dot{\theta}^2 \int \rho r^2 dA + \frac{1}{2} \rho \dot{\theta}'^2 \int \psi^2 dA \right) - \left( \frac{1}{2} C \theta'^2 \right) \right] dz \tag{A.4}$$

Noting that $\int \rho r^2 dA$ is the polar mass moment of inertia, $I_p$, and defining,

$$H = \rho \int \psi^2 dA \tag{A.5}$$

where $H$ is to be determined after $\psi$ has been evaluated (see Timoshenko and Goodier, 1990, p. 295) and $\rho$ is the unit density of the material. The Lagrangian density, $\mathcal{L}$, can be expressed,

$$\mathcal{L} = I_p \dot{\theta}^2 + \frac{1}{2} \dot{\theta}'^2 H - \frac{1}{2} C \theta'^2 \tag{A.6}$$

Integrating by parts and invoking Hamilton's Principle of least action the Euler-Lagrange equation is expressed,

$$I_p \ddot{\theta} - H \ddot{\theta}'' - C \theta'' = 0 \tag{A.7}$$

Seeking a solution of the form $\theta = e^{i\omega t + ikz}$ results in a dispersion equation that relates the torsional wavenumber, *k*, to any frequency, $\omega$.

$$-I_p\omega^2 - Hk^2\omega^2 + Ck^2 = 0 \tag{A.8}$$

Finally, in the low frequency limit, the term in *H* drops out and the speed of the torsional wave, $\frac{\omega}{k}$, can be approximated by,

$$\frac{\omega}{k} \approx \sqrt{\frac{C}{I_p}} \tag{A.9}$$

The static torsional rigidity, *C*, is the ratio of the torque, $M_t$, to the twist, $\theta'$,

$$C = \frac{M_t}{\theta'} \tag{A.10}$$

The membrane analogy equates the magnitude of the shearing stress at any point to twice the integral of the stress function, $\phi$, over the differential area, *dA*.

$$M_t = 2\int \phi dA \tag{A.11}$$

The stress function, $\phi$, is evaluated by solving the Poisson partial differential equation over the cross-section with $\phi = 0$ enforced on the boundaries.

$$\frac{\partial^2\phi}{dx^2} + \frac{\partial^2\phi}{dy^2} = -2G\theta' \tag{A.12}$$

**A.3 Test Procedure**

I modeled unworn 136RE and 115RE rail profiles in Autodesk AutoCAD software based on the AREMA specifications for these rail profiles (L. B. Foster

Company, 2004). Worn 136RE and 115RE profiles (dashed lines) were produced from wear patterns typically seen at the end of a rail's service life.

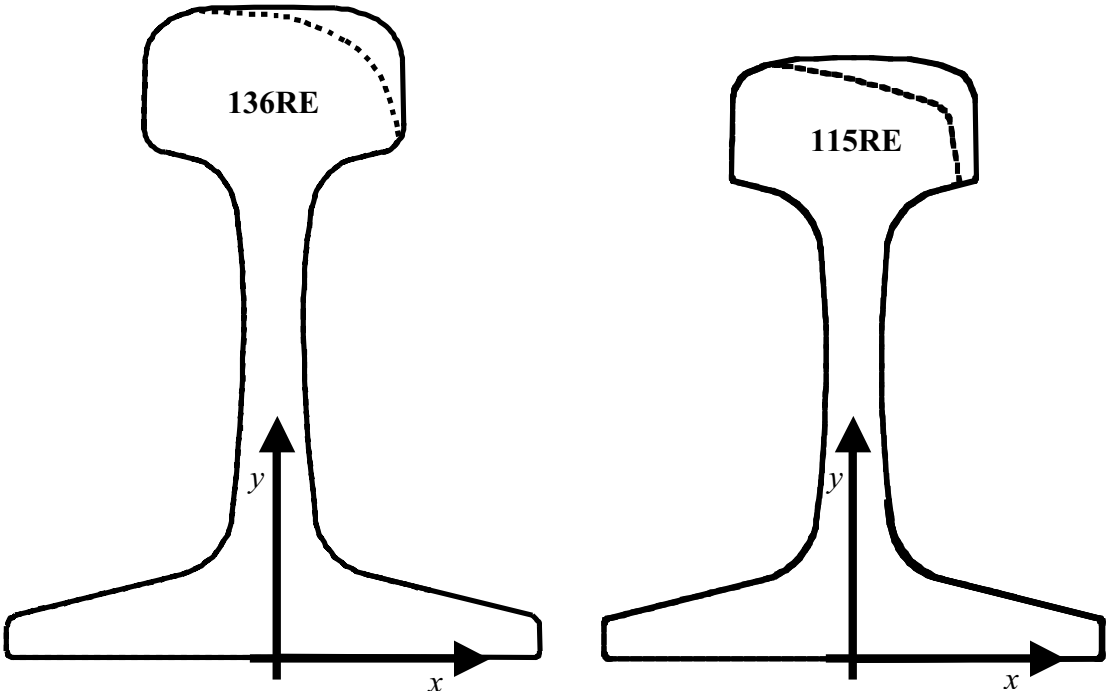


**Figure A.2 Analyzed Rail Profiles**

AutoCAD was also used to calculate the cross-sectional area of each rail profile. The AutoCAD sketch was imported into Autodesk Inventor software and the center of mass was located for each profile.

The profiles were imported one-by-one into the FEMLAB sketch mode and the boundaries constrained against displacement. A refined finite element mesh was created for each profile. Comsol FEMLAB software was used to solve Poisson's partial differential equation (Equation A.12) over the profile's cross-section.

First, a trial with a circular slice with a radius of unity was attempted to confirm the solution to the exact one predicted by St. Venant Torsion Theory. FEMLAB solved the Poisson equation on the circle and similarly the rail profiles. FEMLAB was also used to compute several numerical integrations on each profile.

The results of the computations were tabulated and the values for the torsional rigidity and the polar mass moment of inertia were calculated. The speed of the torsional wave was calculated for all four profiles and the result obtained for unworn 136RE rail was compared to Damljanovic's (2003) finite element predictions for torsional wave speed on unworn 136RE rail.

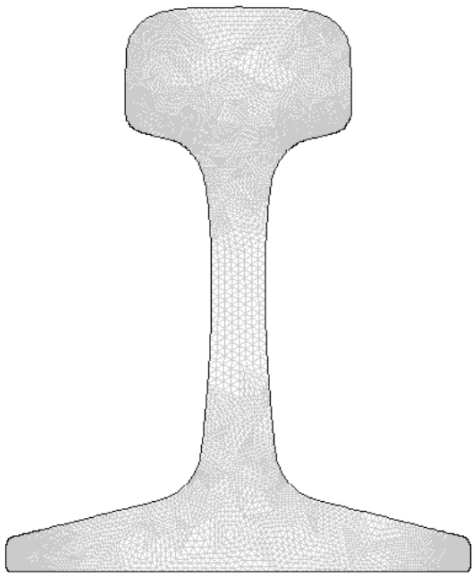

**Figure A.3 Unworn 136RE Finite Element Mesh**

## A.4 Results

The initial verification of the membrane analogy on a unit circle cross-section also involved a look at how quickly the solution converged. The ultimate program run involved a 385,793-element mesh whose integration of the stress function, $\phi$, over the area took more than four minutes. From this investigation it was realized that numeric

solutions of the integration of the stress function sufficiently approach the exact solution with about 70,000 elements in the mesh.

The study of the unit circle is summarized below. The center of mass of the circle was also the origin so applications of the parallel axis theorem were not needed in calculating the mass polar moment of inertia about the center of mass (center of rotation).

| Circular Shaft (1in radius) | |
|---|---|
| Integral $\phi$ ($in^2$) | 0.3927 |
| Area ($in^2$) | 3.1416 |
| $I_{xx}$ ($in^4$) | 0.7854 |
| $I_{yy}$ ($in^4$) | 0.7854 |
| $I_{xx}+I_{yy}$ ($in^4$) | 1.5708 |
| $I_p$ (lb-in) | 1.5708 |
| C (lb-$in^2$/rad) | 1.5708 |

**Table A.1 Circular Shaft Results**

The same values for the circular shaft were obtained as those predicted by the St. Venant torsion theory. Taking $G$ and $\rho$ as unity, the value for the torsional rigidity of the circular shaft was computed as 1.5708. St. Venant torsion theory for the same solid circular shaft states the torsional rigidity should be taken as $GJ$, where $J$ is the polar moment of inertia. For a unit circle $GJ = (1)\frac{\pi r^4}{2} = 1.570796$. As expected, the calculated torsional rigidity using the membrane analogy is equal to that predicted by St. Venant torsion theory.

The investigation on rail profiles first involved using AutoCAD software to sum the area of the cross-section and Inventor software to locate the center of mass from coordinates centered at the middle of the rail base (Figure A.3). The results of these computations are shown in Table A.2.

| Profile | Unworn 136 | Worn 136 | Unworn 115 | Worn 115 |
|---|---|---|---|---|
| Area ($in^2$) | 13.38 | 12.73 | 11.26 | 10.48 |
| $d_x$ (in) | 0.00 | 0.19 | 0.00 | 0.23 |
| $d_y$ (in) | 3.36 | 3.21 | 2.97 | 2.76 |

**Table A.2 Geometric Properties for Studied Rail Profiles**

The value of the x-distance to the center of mass, $d_x$, was nonzero due to the asymmetric wear on the worn profiles. Unworn profile values of $d_y$ were nearly equal to published values (L. B. Foster Company, 2004). FEMLAB computations for the first and second moments of area about the origin were translated to the point of center of mass using the parallel axis theorem. The integral values and values of $I_p$ are tabulated in Table A.3. The density of steel, $\rho_{steel}$, was taken as 7.339E-4 slugs/$in^3$.

| Profile | Unworn 136 | Worn 136 | Unworn 115 | Worn 115 |
|---|---|---|---|---|
| Integral x | 0.0000 | -0.5357 | 0.0000 | -0.5514 |
| Integral y | 44.9181 | 40.7534 | 33.6058 | 28.6020 |
| Integral $x^2$ | 14.5106 | 13.8738 | 10.7301 | 10.1041 |
| Integral $y^2$ | 245.7979 | 216.9490 | 166.3519 | 135.0942 |
| $I_{xx}$ ($in^4$) | 94.7430 | 85.7778 | 67.0286 | 55.2618 |
| $I_{yy}$ ($in^4$) | 14.5106 | 13.4142 | 10.7301 | 9.5497 |
| $I_{xx}+I_{yy}$ ($in^4$) | 109.2537 | 99.1920 | 77.7587 | 64.8115 |
| $I_p$ (lb-in) | 0.0802 | 0.0728 | 0.0571 | 0.0476 |

**Table A.3 Integral Values for Studied Rail Profiles**

The values of the moment of inertias were within 5% of the handbook values for unworn 136RE and unworn 115RE rail (L. B. Foster Company, 2004). $I_{xx}$ and $I_{yy}$ were summed to calculate the polar moment of inertia, $I_{xx}+I_{yy}$. The mass polar moment of inertia, $I_P$, was calculated by multiplying the density, $\rho$, and $I_{xx}+I_{yy}$.

The integral of the stress function for each membrane was computed and a numerical value for the torsional rigidity, C, calculated taking $G$ as 11,240 lb/in$^2$.

| Profile | Unworn 136 | Worn 136 | Unworn 115 | Worn 115 |
|---|---|---|---|---|
| Elements | 67200 | 67904 | 80384 | 73920 |
| DOF | 135697 | 137113 | 162241 | 149225 |
| Time for Solution (sec) | 21.0 | 45.9 | 25.8 | 23.4 |
| Integral $\phi$ (in$^2$) | 1.6321 | 1.4188 | 1.2273 | 0.8947 |
| C (lb-in$^2$/rad) | 73379 | 63789 | 55179 | 40224 |

**Table A.4 Torsional Rigidity of Studied Rail Profiles**

The torsional wave speed was calculated last. Wear on both the 136RE and 115RE rail profiles changed the torsional wave speed by less than 7 percent.

| Profile | Unworn 136 | Worn 136 | Unworn 115 | Worn 115 |
|---|---|---|---|---|
| Wave Speed | 957 | 936 | 983 | 920 |
| Percent Change | 2.1 | | 6.5 | |

**Table A.5 Torsional Wave Speed and Percent Change due to Wear**

The calculated speed of the unworn 136 torsion wave was compared to finite element predictions by Damljanovic (2003). There was nearly a 30 percent difference of wave speed between those predicted by the membrane analogy and the ones predicted by Damljanovic (2003).

| Profile | Unworn 136 |
|---|---|
| Wave speed as predicted by Membrane Analogy | 957 |
| Wave Speed as Predicted by Damljanovic (2003) FEA | 1230 |
| Percent Difference | 28.6 |

**Table A.6 Membrane Analogy and FEA Comparison**

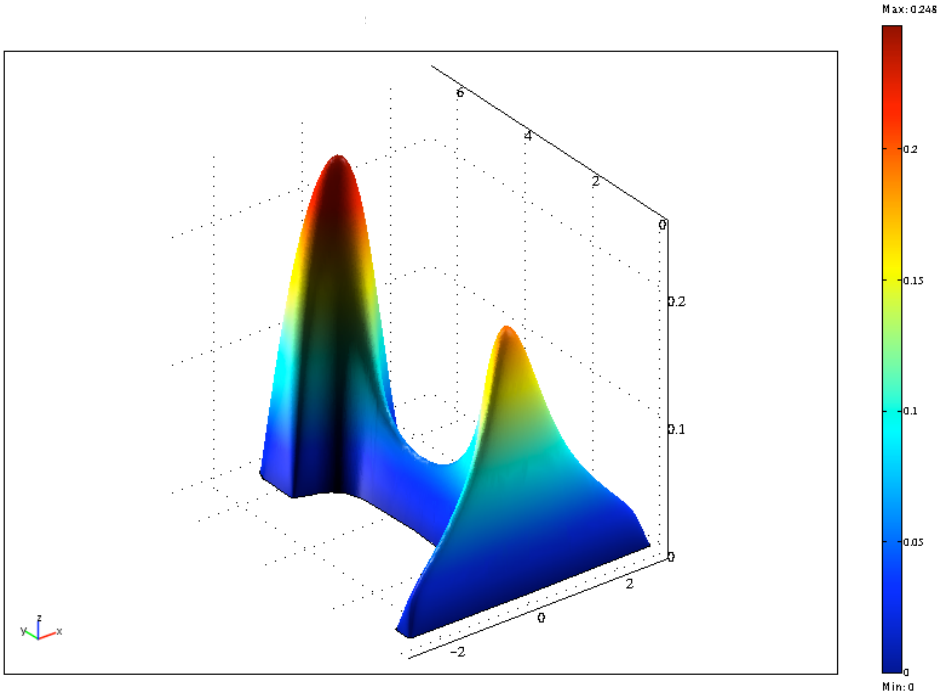


**Figure A.4 Expanded Membrane for Worn 115RE Rail**

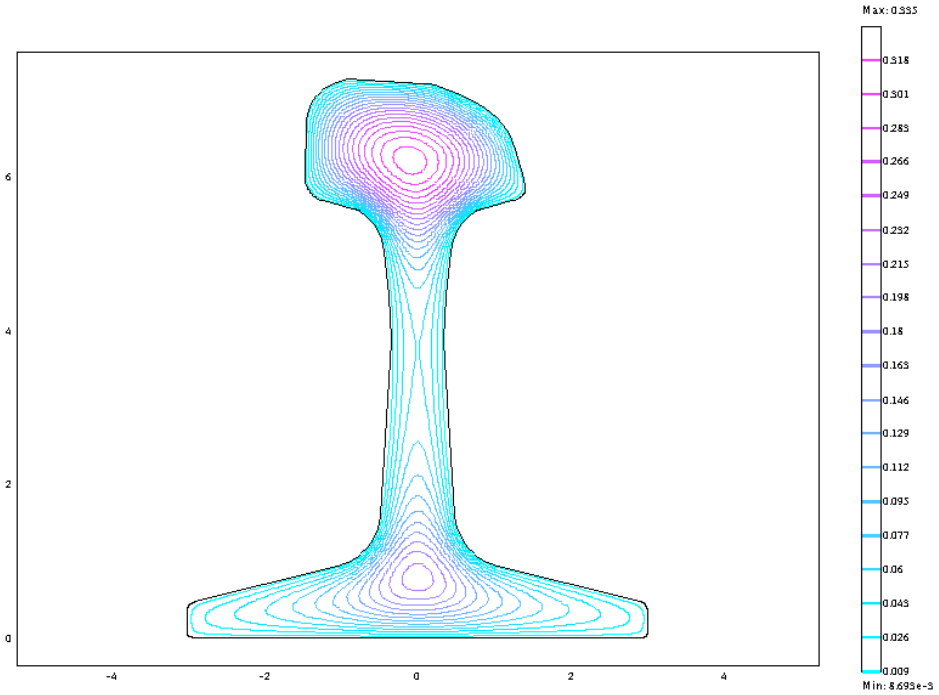


**Figure A.5 Contour Map of ϕ for Worn 115RE Rail**

## A.5 Conclusions

The torsional wave speed can be predicted with sufficient accuracy without rail profilometry because torsional wave speeds as predicted by the membrane analogy were observed to change less than 10% with high degrees of wear. Worn rail profiles resulted in a 2.1% difference in torsional wave speed from the unworn profile in 136RE rail, and 6.5% in 115RE rail. Simple measurements of the rail profile in the field would help improve accuracy of torsional wave speed guesses. The results suggest that the change in torsional wave speed is small even when the rail is very worn. However, to obtain an accurate value of torsional wave speed the profile of the rail should be determined near the laser vibrometry application and membrane analogy of elasticity used.

There still exists a need to study the trend of the torsional wave speed as a function of the degree of wear. This study investigated the extreme cases, unworn and worn, but the change with respect to degree of wear is not yet known.

# REFERENCES


American Railway Engineering and Maintenance-of-Way Association (AREMA) (2000) *AREMA Manual for Railway Engineering*, Landover, MD, Part 5-Track.

Anderson, R. T., & C. P. L. Barkan. (2003) Railroad Accident Rates for Use in Transportation Risk Analysis, *Transportation Research Record: Journal of the Transportation Research Board*, No. 1863, pp. 88-98.

Association of American Railroads (1978) *Analysis of Class I Railroads*. Association of American Railroads, Washington, D.C.

Association of American Railroads (2003) *Analysis of Class I Railroads*. Association of American Railroads, Washington, D.C.

Banas, G. & C. Simsir. (2002) *Strain Gauges: Theory, Instrumentation and Installation, 2nd edition*, University of Illinois College of Engineering, Urbana, IL.

Béliveau, J. G., & T. M. Murray. (1996) *Lateral Vibration of #115 Rail for Axial Compression up to 100 Kips, CE/VPI-ST96/03*, Virginia Polytechnic Institute & State University, Blacksburg, VA.

Boggs, T. P., J. G. Béliveau, & T. M Murray. (1994) *Determination of Axial Load and Support Stiffness of Continuous Beams by Vibration Analysis, CE/VPI-ST94/14*, Virginia Polytechnic Institute & State University, Blacksburg, VA.

Damljanovic, V. (2003) *Guided Waves Technique for Measurement of Contained Stress in Uniform Slender Elastic Bodies, Ph.D. Thesis*, University of Illinois at Urbana-Champaign Department of Theoretical and Applied Mechanics, Urbana, IL.

Davis, D. (2004, May) Principal Researcher, Transportation Technology Center, Inc. Personal Communication.

Graff, K. F. (1975) *Wave Motion in Elastic Solids*, Ohio State University Press, Columbus, OH.

Green, J. & P. Shrubsall. (2004) Management of Neutral Rail Temperature, *In: Proceedings of the 2004 Annual Conference, American Railway Engineering and Maintenance of Way Association*, Landover, MD.

Guilloteau, S. (2000) (ed.) The Interferometer Principles, *Proceedings of the 2000 IRAM Millimter Interferometry Conference*, Cedex, France.

Hauk, V. (1997) *Structural and Residual Stress Analysis by Nondestructive Methods*, Elsevier Science B.V., Amsterdam.

Hay, W. (1982) *Railroad Engineering*, John Wiley & Sons, New York, NY.

Kish, A., S. Kalay, A. Hazell, J. Schoengart, & G. Samavedam. (1993) Rail Longitudinal Force Measurement Evaluation Studies Using the Track Loading Vehicle, *American Railway Engineering Association Bulletin*, No. 742, pp. 315-342.

Kish, A., & G. Samavedam. (1987) Longitudinal Force Measurement in Continuous Welded Rail from Beam Column Deflection Response, *American Railway Engineering Association Bulletin*, No. 712, pp. 280-301.

Kish, A., & G. Samavedam. (2005) Improvements In CWR Destressing for Better Management of Rail Neutral Temperature, *In: Proceedings of the 2005 Annual Conference, Transportation Research Board*, Washington, D.C.

Kish, A., G. Samavedam, & D. Jeong. (1987) The Neutral Temperature Variation of Continuous Welded Rails, *American Railway Engineering Association Bulletin*, No. 712, pp. 257-279.

L. B. Foster Company. (2004) *Foster Rail Products*, Pittsburgh, PA.

Lees, H. Jr. (2005, March) Senior Engineer Track and Structures, Technical Research and Development, BNSF Railway. Personal Communication.

Livingston, T., J. G. Béliveau, & D. R. Huston. (1995) Estimation of Axial Load in Prismatic Members Using Flexural Vibrations, *Journal of Sound and Vibration*, Vol. 179, No. 5, pp. 899-908.

Lo, C. C. H., J. A. Paulsen, E. R. Kinser, & D. C. Jiles. (2004) Quantitative Evaluation of Stress Distribution in Magnetic Materials by Barkhausen Effect and Magnetic Hysteresis Measurements, *IEEE Transactions on Magnetics*, Vol. 40, No. 4, pp. 2173-2175.

Meador, B. (2004) CN Railway. Track Destressing Workshop held in Urbana, IL, 4 November 2004.

Read, D., A. Kish, & J. Lopresti. (2004) Management of Longitudinal Forces under Heavy Axle Loads, *In: Proceedings of the 2004 Annual Conference, American Railway Engineering and Maintenance of Way Association*, Landover, MD.

Schmidt, E. (2005, August) Chief Operator, Sperry Rail Service. Personal Communication.

Selig, E. T. & J. M. Waters. (1994) *Track Geotechnology and Substructure Management*, Thomas Telford, London.

Si-Chaib, M.O., S. Menad, H. Djelouah, & M. Bocquet (2001) An Ultrasound Method for the Acoustoelastic Evaluation of Simple Bending Stresses, *NDT&E International*, No. 34, pp.521-529.

Szelazek, J. (1998) Monitoring of Thermal Stresses in Continuously Welded Rails with Ultrasonic Technique, *NDTnet*, Vol. 3, No. 6, pp. 1-8.

Timoshenko, S. P., & J. N. Goodier. (1970) *Theory of Elasticity*, McGraw-Hill, New York, NY.

Tsuchida, Y., & M. Enokizono. (2003) Stress Evaluation by Chaotic Characteristic of Barkhausen Noise, *In: Proceedings of the 2003 Annual Conference, American Institute of Physics*, College Park, MD.

Tuckett, J. (2005, July) Track Supervisor, CN Railway. Personal Communication.

Vortok International & AEA Technology. (2004) *An Operator's Guide to VERSE® United Kingdom Version*, AEA Technology, London.

Weaver, R. & C. Barkan (2000) Vibration Measurements of Rail Stress, *Transportation Research Board High-Speed Rail – Innovations Deserving Exploratory Analysis Program.* Stage 1 Proposal.

Weaver, W. Jr., S. P. Timoshenko, & D. H. Young. (1990) *Vibration Problems in Engineering, 5th Edition.* John Wiley and Sons, Inc., New York, NY.

Wegner, A. (2005) Non-Destructive Determination of the Stress Free Temperature in CWR Tracks, *In: Proceedings of the 2005 Longitudinal Force Workshop* (Compact Disk). Pueblo, CO, pp. 173-216.

Zarembski, A. (1980) *On the Nondestructive In-Track Measurement of Longitudinal Rail Forces, R-406*, Association of American Railroads, Chicago, IL.

Zarembski, A., G. Grissom, & H. Lees, Jr. (2004) Development of Track Buckling Risk Analysis Methodology, *In: Proceedings of the 2004 Annual Conference, American Railway Engineering and Maintenance of Way Association*, Landover, MD.

# AUTHOR'S BIOGRAPHY

Michael J. Koob was born July 9, 1982, in Lake Forest, Illinois. He discovered his interests in engineering and transportation at a young age. During high school he worked as a technician at Wiss Janney Elstner Associates (WJE) in Northbrook, Illinois and spent his summer earnings financing his flying lessons. He obtained his private pilot license and instrument rating at age seventeen and commercial license at age eighteen before coming to the University of Illinois at Urbana-Champaign.

Koob entered the Institute of Aviation at the University of Illinois at Urbana-Champaign in August of 2000 focused on a career in aviation. While at the institute he earned his flight instructor and multiengine certificates and completed his AVIPC in the spring of 2001. His experiences with WJE and the advice of his father, however, persuaded him to "get a backup" in civil engineering. He graduated from the department of civil engineering with honors in the fall of 2003.

Koob has remained active as a commercial pilot and flight instructor during his five years at the University. He has logged nearly six hundred flight hours as a flight instructor and hundreds more flying skydivers and towing gliders. He has built engineering experience by interning summers with WJE and recently completed practical training with the Swiss highway department. Following the completion of his Master of Science degree he will accept an engineering position with WJE in Denver, Colorado while hoping for the chance to join the ranks as an Air National Guardsman.